A Direct Method for Bloch Wave Excitation by Scattering at the Edge of a Lattice

University of Liverpool

Rachel Brougham

March 14, 2018

Abstract

A new method for calculating the reflection and transmission properties of lattices is developed and demonstrated for the case of a semi-infinite lattice of sound-hard and sound-soft acoustic scatterers. Both point-scatterers and finite-sized scatterers are considered, with generalisation from the former to the latter being considerably simpler than previous approaches to this problem.

Contents

1 Introduction

A Bloch wave is a type of wave that propagates through a periodically-repeating structure without loss of energy, and has applications in a range of physical contexts such as electromagnetic waves in photonic crystals, or acoustic waves in phononic crystals. The existence of Bloch waves in a medium depends on the so-called "band-structure" of the medium, i.e. the physical properties of the structure dictate whether or not the propagation of Bloch waves is possible. The parameters governing the problem, such as frequency and lattice geometry, may lie in a:

- Stop band- where no propagation is possible
- Partial stop band- where propagation is possible, dependent on direction
- Pass band- where propagation is possible in all directions

Consequently, one can achieve unusual effects such as filtering or guiding waves using lattice structures; this idea underpins the design of photonic crystals and metamaterials. For example, [12] studies electromagnetic waves propagating through a periodic array of cylinders, and the results demonstrate parameter regimes for which Bloch wave propagation is permitted. This has implications for designing a band gap filter, although further information about Bloch amplitudes would be required. Phononic crystals are acoustic metamaterials that may have a band gap that prevents acoustic waves of certain frequencies from being transmitted, and have been studied experimentally in two-dimensions [7] and three-dimensions [4]. Photonic metamaterials and fabricated photonic crystals interact with light waves, and hence have applications in transformation optics [2].

Most existing literature on Bloch waves is concerned with the propagation problem, which consists of determining the possibility of Bloch waves *existing* in a medium, but this yields no information about amplitudes of the waves.

The excitation problem is concerned with the incidence of a wave upon a periodic lattice of identical cylinders, and determining the reflection and transmission properties of the structure. We can hence determine the proportion of energy that may be converted into Bloch waves (i.e. the amplitudes of any Bloch waves that may be excited).

Although the propagation problem has been studied extensively, the excitation problem has received far less attention, and is generally a more difficult problem. Literature concerned with the excitation problem uses the Wiener-Hopf method, which is typically used to account for sharp changes in boundary conditions, for example a barrier that occupies the half-line $y = 0, \quad x > 0$ as in [13]. The method was adapted in [6] to account for semi-infinite array problems, and so is a natural choice for problems of this type. The excitation problem is addressed in [18] for point-scatterers, i.e. a lattice of identical cylinders whose radius is asymptotically small compared with all other parameters. This work is continued in [19] by increasing the radius of the cylinders (which corresponds to increasing the frequency). In both of these papers, the wave field is represented in terms of multipole expansions, to which Graf's Addition Theorem [11] is applied to obtain infinite non-convergent systems of equations, and z transforms are then used to convert these systems into Wiener-Hopf equations. For the point-scatterer case, the Wiener-Hopf equation is scalar, and therefore straight-forward to solve numerically. The introduction of "finite-size effects" in [19] leads to a matrix Wiener-Hopf equation, and no general method for solving such equations exists. For the excitation problem discussed in Section 3.2, there is an approximate method described in [19], but it is complicated, and difficult to implement.

To avoid the difficulty associated with introducing finite-size effects, the following uses the filtering technique developed in [10] to remove non-convergent terms from the multipole expansions. The resulting infinite system is therefore

convergent, and can be solved by truncation.

We will be considering acoustic waves, and developing a method that is more direct and generalisable to calculate the reflection and transmission properties of lattices. The method will first be developed for point-scatterers, and then generalised to account for finite-size effects, with more involved algebra being the only increased difficulty. The methods demonstrated here could be further generalised to account for different shaped scatterers, three-dimensional lattices, water waves, or flexural waves in thin plates. For the three-dimensional case, research into Bloch wave excitation in a lattice of nanospheres was conducted in [1], and so this could be extended to include finite-sized spheres. Literature such as [5] and [3] on waves interacting with lattice structures in thin plates is also only concerned with point-scatterers. Using the new method, one could easily incorporate finite-size effects.

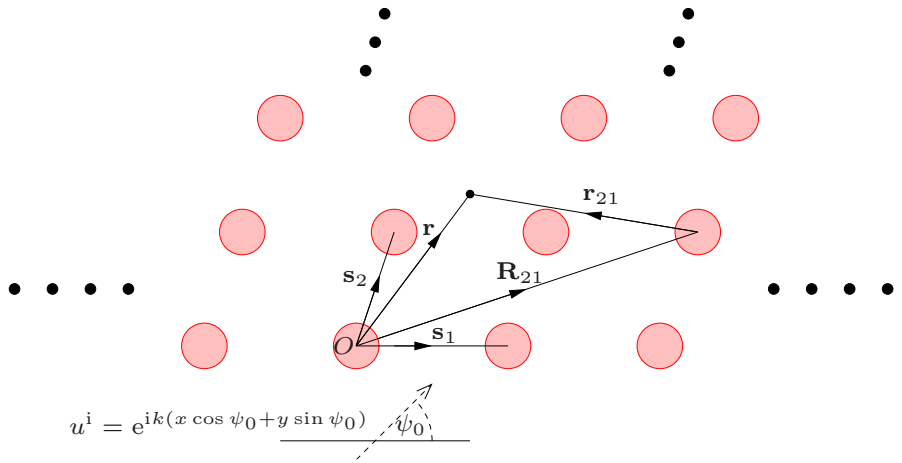

Figure 1: Geometry and notation for scattering by a semi-infinite lattice

2 Formulation of the Problem

2.1 The Boundary Value Problem

Consider the interaction of acoustic wave fields $u(\mathbf{r})$ with a ltwo-dimensional lattice consists of identical cylinders with position vectors $\mathbf{R}_{jp}$ such that $\mathbf{R}_{jp} = j\mathbf{s}_1 + p\mathbf{s}_2$, for two linearly independent vectors $\mathbf{s}_1 = [s_1, 0]$, $\mathbf{s}_2 = [\eta_1, \eta_2]$ in the (x, y)-plane (see figure 1). Here, wave motion is time-harmonic, and so solutions to the wave equation

$$\nabla^2 U(\mathbf{r}, t) - \frac{1}{c^2} U_{tt}(\mathbf{r}, t) = 0 \tag{1}$$

take the form

$$U(\mathbf{r}, t) = u_1(\mathbf{r}) \cos(\omega t) + u_2(\mathbf{r}) \sin(\omega t), \tag{2}$$

where c is wave-speed and ω is the frequency. Differentiating (2) twice with respect to time, we see that

$$U_{tt} = -\omega^2 U, \tag{3}$$

and so time-harmonic wave motion satisfying (1) also satisfies

$$(\nabla^2 + k^2) u(\mathbf{r}) = 0, \qquad k = \frac{\omega}{c}. \tag{4}$$

This is the two-dimensional Helmholtz equation, and is the governing equation for our problem, with c the speed of sound. Note that once the complex-valued function $u(\mathbf{r})$ has been determined, a time-harmonic acoustic potential can be retrieved by writing

$$U(\mathbf{r}, t) = \Re[u(\mathbf{r})e^{-i\omega t}]. \tag{5}$$

On the surface of each cylinder, the field satisfies the Dirichlet boundary condition,

$$u(\mathbf{r}) = 0 \tag{6}$$

for sound-soft surfaces, and the Neumann boundary condition

$$\frac{\partial u}{\partial n} = \mathbf{n} \cdot \nabla u = 0 \tag{7}$$

for sound-hard surfaces.

We will consider fields satisfying the one- and two-dimensional quasiperiodicity properties, given by

$$u(\mathbf{r} + s_1\hat{\mathbf{x}}) = e^{is_1\beta_x}u(\mathbf{r}) \tag{8}$$

and

$$u(\mathbf{r} + \mathbf{R}_{jp}) = e^{i\mathbf{R}_{jp}\cdot\boldsymbol{\beta}}u(\mathbf{r}) \tag{9}$$

respectively, where β is defined in Section 2.3

2.2 Solution to the Helmholtz equation

Since we are dealing with scattering by circular cylinders, it is useful to obtain the solution in polar coordinates. The Helmholtz equation is therefore given by

$$\left(\frac{\partial^2}{\partial r^2} + \frac{1}{r}\frac{\partial}{\partial r} + \frac{1}{r^2}\frac{\partial^2}{\partial \theta^2} + k^2\right) u(r, \theta) = 0, \tag{10}$$

which can be solved using separation of variables by writing

$$u(r, \theta) = R(r)\Theta(\theta), \tag{11}$$

and inserting this into (10) to obtain

$$R''\Theta + \frac{1}{r}R'\Theta + \frac{1}{r^2}R\Theta'' + k^2 R\Theta = 0. \tag{12}$$

Multiplying by $\frac{r^2}{R\Theta}$ yields

$$r^2\frac{R''}{R} + r\frac{R'}{R} + r^2k^2 = -\frac{\Theta''}{\Theta}. \tag{13}$$

The left- and right-hand sides of this equation are independent, and therefore must equal a constant. Since $\Theta(\theta)$ must be 2π periodic, let

$$\frac{\Theta''}{\Theta} = -n^2 \qquad n \in \mathbb{Z} \tag{14}$$

so that

$$\Theta(\theta) = C_1\cos(n\theta) + C_2\sin(n\theta). \tag{15}$$

For the left-hand side of (13), we have

$$r^2R'' + rR' + (r^2k^2 - n^2)R = 0. \tag{16}$$

This is Bessel's equation and has two independent solutions,

$$R(r) = J_n(kr), \qquad \text{and} \qquad R(r) = Y_n(kr), \tag{17}$$

i.e. the Bessel function and Neumann function of order n (respectively). Thus, the general solution is

$$u(r,\theta) = \sum_{n=0}^{\infty}[A_n\cos(n\theta) + B_n\sin(n\theta)]J_n(kr) + [D_n\cos(n\theta) + E_n\sin(n\theta)]Y_n(kr), \tag{18}$$

or, by defining

$$J_{-n} = (-1)^n J_n \quad \text{and} \quad Y_{-n} = (-1)^n Y_n,$$

we have

$$u(r,\theta) = \sum_{n=-\infty}^{\infty}[E_nJ_n(kr) + F_nY_n(kr)]e^{in\theta}. \tag{19}$$

Next, we must ensure that our calculations are physically viable in that energy radiated from the incident field is scattered *to* infinity, and that no scattered energy is incoming *from* infinity. We therefore impose the Sommerfeld radiation condition [15], given by

$$\sqrt{r}\left(\frac{\partial u}{\partial r} - iku\right) \to 0 \quad \text{as} \quad r \to \infty, \tag{20}$$

which guarantees that our solution is unique and physical (for details on this, see [11]).

We have

$$\begin{aligned}\sqrt{r}\left(\frac{\partial u}{\partial r} - iku\right) &= k\sqrt{r}\sum_{n=-\infty}^{\infty}[E_nJ_n'(kr) + F_n(kr)Y_n'(kr) - iE_nJ_n(kr) - iF_nY_n(kr)]e^{in\theta} \\ &= \frac{k\sqrt{r}}{2}\sum_{n=-\infty}^{\infty}[E_n(J_{n-1}(kr) - J_{n+1}(kr) - 2iJ_n(kr)) \\ &\quad + F_n(Y_{n-1}(kr) - Y_{n+1}(kr) - 2iY_n(kr)]e^{in\theta}, \end{aligned} \tag{21}$$

where we have used the fact that

$$J_n'(z) = \frac{1}{2}(J_{n-1}(z) - J_{n+1}(z)), \qquad Y_n'(z) = \frac{1}{2}(Y_{n-1}(z) - Y_{n+1}(z)).$$

Now we use the asymptotic formulas [14],

$$J_n(z) \sim \sqrt{\frac{2}{\pi z}}\cos(z - \frac{\pi}{4}(2n+1)) \quad \text{and} \quad Y_n(z) \sim \sqrt{\frac{2}{\pi z}}\sin(z - \frac{\pi}{4}(2n+1))$$

as $z \to \infty$, and in this way we find that

$$\sqrt{r}\left(\frac{\partial u}{\partial r} - iku\right) \sim \sqrt{\frac{k}{2\pi}} \sum_{n=-\infty}^{\infty} [E_n(\cos(kr - \frac{\pi}{4}(2n-1)) - \cos(kr - \frac{\pi}{4}(2n+3)) \tag{22}$$

$$\begin{aligned}
&- 2i\cos(kr - \frac{\pi}{4}(2n+1)) + F_n(\sin(kr - \frac{\pi}{4}(2n-1)) \\
&- \sin(kr - \frac{\pi}{4}(2n+3)) - 2i\sin(kr - \frac{\pi}{4}(2n+1))]e^{in\theta} \\
&= \sqrt{\frac{k}{2\pi}} \sum_{n=-\infty}^{\infty} [E_n(\cos(\beta + \frac{\pi}{2}) - \cos(\beta - \frac{\pi}{2}) - 2i\cos(\beta)) \\
&+ F_n(\sin(\beta + \frac{\pi}{2}) - \sin(\beta - \frac{\pi}{2}) - 2i\sin(\beta))]e^{in\theta} \\
&= \sqrt{\frac{2k}{\pi}} \sum_{n=-\infty}^{\infty} [-iE_n(\cos(\beta) - i\sin(\beta) + F_n(\cos(\beta) - i\sin(\beta))]e^{in\theta} \\
&= \sqrt{\frac{2k}{\pi}} [e^{-i\beta} \sum_{n=-\infty}^{\infty} (-iE_n + F_n)]e^{in\theta}, \qquad (23)
\end{aligned}$$

where $\beta = kr - \frac{\pi}{4}(2n+1)$. Thus, (19) satisfies the Sommerfeld radiation condition (20) if and only if

$$F_n = iE_n.$$

The general solution hence takes the form

$$\begin{aligned}
u(r) &= \sum_{n=-\infty}^{\infty} [E_n J_n(kr) + iE_n Y_n(kr)]e^{in\theta} \qquad (24) \\
&= \sum_{n=-\infty}^{\infty} E_n H_n^{(1)}(kr)e^{in\theta}, \qquad (25)
\end{aligned}$$

where $H_n^{(1)}$ is the nth order Hankel function of the first kind, defined as

$$H_n^{(1)}(kr) = J_n(kr) + iY_n(kr).$$

Throughout our calculations, we will be using the notation

$$\mathcal{J}_n(\mathbf{r}) = e^{in\theta} J_n(kr) \tag{26}$$

and

$$\mathcal{H}_n(\mathbf{r}) = e^{in\theta} H_n^{(1)}(kr). \tag{27}$$

2.3 Grating modes

Any field satisfying the one-dimensional quasiperiodicity property (8) and the Helmholtz equation can be expanded as a series of grating modes, i.e.

$$u(\mathbf{r}) = \sum_{j=-\infty}^{\infty} e^{i\beta_{xj}x} \left[c_j^- e^{\gamma(\beta_{xj})y} + c_j^+ e^{-\gamma(\beta_{xj})y} \right], \tag{28}$$

where $\beta_{xj} = \beta_x + 2j\pi/s_1$ and γ is a function such that

$$\gamma(t) = \begin{cases} \sqrt{t^2 - k^2} & \text{if} \quad |t| \geq |k|, \\ -i\sqrt{k^2 - t^2} & \text{if} \quad |k| < |t|. \end{cases} \tag{29}$$

Here, c_j^+ and c_j^- are the amplitude coefficients of upward and downward propagating modes respectively, so that modes with coefficients c_j^+ propagate in the positive y direction. Terms in (28) for which the real part of $\gamma(\beta_{xj})$ is zero correspond to propagating modes, and so let us define the sets

$$\mathcal{M} = \{j : \quad j \in \mathbb{Z}, \quad |\beta_{xj}| \leq k\}, \qquad \mathcal{N} = \{j : \quad j \in \mathbb{Z}, \quad |\beta_{xj}| > k\}. \tag{30}$$

For the purpose of the propagation problem discussed in Section 3.1, it is useful to determine the direction in which energy is transported across lines parallel to the x-axis. It is shown in [8] that the amount of energy transported over a line S in one time-period can be calculated using the line integral

$$\langle E_S \rangle = -\frac{P_0\omega}{2} \Im \int_S u(\mathbf{r}) \frac{\partial}{\partial n} u^*(\mathbf{r}) \, \mathrm{d}s, \tag{31}$$

where P_0 is the undisturbed fluid density. If $\langle E_S \rangle > 0$, then energy is transported in the direction of the normal n. Thus, taking S to be the line joining the points

$(x_0 - s_1/2, y_0)$ and $(x_0 + s_1/2, y_0)$ and the normal to be parallel to the y-axis gives

$$\langle E_S \rangle = -\frac{P_0\omega}{2}\Im \int_{x_0-s_1/2}^{x_0+s_1/2} u(\mathbf{r})\frac{\partial}{\partial y}u^*(\mathbf{r})\bigg|_{y=y_0} \mathrm{d}x, \tag{32}$$

or, after utilising the orthogonality condition

$$\int_{x_0-s_1/2}^{x_0+s_1/2} e^{i\beta_{xj}x}e^{-i\beta_{xp}x}dx = s_1\delta_{jp}, \tag{33}$$

we obtain

$$\langle E_S \rangle = -\frac{P_0\omega s_1}{2}\Im \sum_{j=-\infty}^{\infty} \gamma^*(\beta_{xj}) \left[c_j^- e^{\gamma(\beta_{xj})y_0} + c_j^+ e^{-\gamma(\beta_{xj})y_0}\right] \left[(c_j^-)^* e^{\gamma(\beta_{xj})^* y_0} - (c_j^+)^* e^{-\gamma(\beta_{xj})^* y_0}\right]. \tag{34}$$

Finally, we can separate terms with $\gamma(\beta_{xj})$ real from those with $\gamma(\beta_{xj})$ imaginary to simplify this to

$$\langle E_S \rangle = \frac{P_0\omega s_1}{2} \sum_{j\in\mathcal{M}} |\gamma(\beta_{xj})|(|c_j^+|^2 - |c_j^-|^2) - P_0\omega s_1 \sum_{j\in\mathcal{N}} \gamma(\beta_{xj})\Im[c_j^+(c_j^-)^*]. \tag{35}$$

2.4 Quasiperiodic Green's Functions

A Green's function is the impulse response of a linear differential equation, i.e. the Green's function $G_0(\mathbf{x}, \boldsymbol{\xi})$ of a linear differential operator $\mathcal{L}$ is a solution to

$$\mathcal{L}G_0(\mathbf{x}, \boldsymbol{\xi}) = \delta(\mathbf{x} - \boldsymbol{\xi}) \qquad x \in \Omega \subset \mathbb{R}^n, \tag{36}$$

where δ is the Dirac delta function such that

$$\delta(\mathbf{Y}) = 0 \quad \text{unless} \quad \mathbf{Y} = 0, \tag{37}$$

and

$$\int_\Omega f(\mathbf{x})\delta(\mathbf{x} - \boldsymbol{\xi})\underset{\sim}{\mathrm{x}} = \begin{cases} f(\boldsymbol{\xi}) & \text{if } (\boldsymbol{\xi}) \in \Omega \\ 0 & \text{otherwise.} \end{cases} \tag{38}$$

When periodicity arises, such as acoustic waves propagating through a periodic structure, the Green's function will be a sum over a lattice of the form [9]

$$G = \sum_{\mathbf{R_j p}\in\Lambda} \mu_j G_0(\mathbf{r}, \mathbf{R}_{jp}),$$

where Λ is the set of all lattice points. If we take $\mu_j = e^{i\boldsymbol{\beta}\cdot\mathbf{R_j}}$ where $\boldsymbol{\beta}$ is a real vector, the result is a phased array of free space Green's functions known as a quasi-periodic Green's function.

To obtain the quasi-periodic Green's function for the Helmholtz equation, we therefore use (24) to find the function satisfying (36). Hence, for a row of cylinders centred at points with position vectors $\mathbf{R}_{jq}$, the quasiperiodic Green's function is given by

$$G_n(\mathbf{r}, \beta_x) = \sum_{j=-\infty}^{\infty} e^{ijs_1\beta_x} \mathcal{H}_n(\mathbf{r} - \mathbf{R}_{j0}), \tag{39}$$

whereas for rows q_0 to q_1 we have

$$G_n^{(q_0,q_1)}(\mathbf{r}, \boldsymbol{\beta}) = \sum_{q=q_0}^{q_1} \sum_{j=-\infty}^{\infty} e^{i\mathbf{R}_{jq}\cdot\boldsymbol{\beta}} \mathcal{H}_n(\mathbf{r} - \mathbf{R}_{jq}). \tag{40}$$

These representations for the Quasi-periodic Green's functions are very slowly-convergent and hence are impractical for computations, but can be converted into rapidly-convergent series by applying the Poisson summation formula [17], given by

$$\sum_{j=-\infty}^{\infty} e^{-ijX} = 2\pi \sum_{j=-\infty}^{\infty} \delta(X - 2j\pi), \qquad X \in \mathbb{R}, \tag{41}$$

to the integral representation of $\mathcal{H}_n$, i.e.

$$\mathcal{H}_n = \frac{-ie^{-i\pi n/2}}{\pi} \int_{-\infty}^{\infty} e^{-\gamma(t)|y| - ixt} \frac{dt}{\gamma(t)} \tag{42}$$

and inserting this into (39) and (40). Hence, the spectral forms of the quasi-periodic Green's functions are given by

$$G_n(\mathbf{r}, \beta_x) = \frac{2(-i)^{n+1}}{s_1} \sum_{j=-\infty}^{\infty} \frac{e^{i\beta_{xj}x - \gamma(\beta_{xj})|y|}}{\gamma(\beta_{xj})} \left[\frac{k}{\beta_{xj} + \gamma(\beta_{xj})}\right]^{n\mathrm{sgn}(y)}, \tag{43}$$

and

$$G_n^{(q_0,q_1)}(\mathbf{r},\boldsymbol{\beta}) = \frac{2(-i)^{n+1}}{s_1}\sum_{j=-\infty}^{\infty}\frac{e^{i\beta_{xj}\mp\gamma(\beta_{xj})y}}{\gamma(\beta_{xj})}\left[\frac{k}{\beta_{xj}\pm\gamma(\beta_{xj})}\right]^n\frac{e^{q_0w_j^{\pm}}-e^{(1+q_1)w_j^{\pm}}}{1-e^{w_j^{\pm}}} \tag{44}$$

where

$$w_j^{\pm} = \pm\eta_2\gamma(\beta_{xj}) + i(\eta_2\beta_y - 2j\pi\eta_1/s_1) \tag{45}$$

and the upper and lower signs are to be taken when $y \geq q_1\eta_2$ and $y \leq q_0\eta_2$ (so that the observer is located above or below an array) respectively. For semi-infinite lattices [18], we have

$$G_n^{(q_0,\infty)}(\mathbf{r},\boldsymbol{\beta}) = \frac{2(-i)^{n+1}}{s_1}\sum_{j=-\infty}^{\infty}\frac{e^{i\beta_{xj}+\gamma(\beta_{xj})y}}{\gamma(\beta_{xj})}\left[\frac{k}{\beta_{xj}-\gamma(\beta_{xj})}\right]^n\frac{e^{q_0w_j^{-}}}{1-e^{w_j^{-}}} \qquad y \leq q_0\eta_2, \tag{46}$$

and

$$G_n^{(-\infty,q_1)}(\mathbf{r},\boldsymbol{\beta}) = \frac{2(-i)^{n+1}}{s_1}\sum_{j=-\infty}^{\infty}\frac{e^{i\beta_{xj}-\gamma(\beta_{xj})y}}{\gamma(\beta_{xj})}\left[\frac{k}{\beta_{xj}+\gamma(\beta_{xj})}\right]^n\frac{e^{q_1w_j^{+}}}{1-e^{-w_j^{+}}} \qquad y \geq q_1\eta_2. \tag{47}$$

Note that (40) satisfies the relationship

$$G_n^{(q_0,q_1)}(\mathbf{r},\boldsymbol{\beta}) = \sum_{q=q_0}^{q_1} e^{iq\mathbf{s}_2\cdot\boldsymbol{\beta}}G_n(\mathbf{r}-q\mathbf{s}_2,\beta_x). \tag{48}$$

In our calculations, we will sometimes need to consider the effect of a Quasiperiodic Green's function with a single term omitted. In particular, we will be concerned with the limit

$$\sigma_n^{(1)}(\beta_x) = \lim_{r\to 0}\left[G_n(\mathbf{r},-\beta_x) - \mathcal{H}_n(\mathbf{r})\right] \tag{49}$$

This is the Schlömilch series, which is a one-dimensional lattice sum computed in [9] as

$$\sigma_n = \sum_{p=-\infty}^{\infty}{\sum_{j=-\infty}^{\infty}}' e^{i\mathbf{R}_{j0}\cdot\boldsymbol{\beta}}\mathcal{H}_n(\mathbf{R}_{j0}). \tag{50}$$

3 Bloch Waves

3.1 Propagation Problem

Here, we will be investigating the amplitudes of upward- and downward-propagating Bloch waves. This information can then be used to determine the reflection and transmission properties of the excitation problem, since only upward-propagating waves can be transmitted. Now, a Bloch wave that propagates through a two-dimensional lattice of cylinders as in figure 1 takes the form

$$u^b(\mathbf{r}) = \sum_{n=-\infty}^{\infty} B_n G_n^{(-\infty,\infty)}(\mathbf{r}, \boldsymbol{\beta}), \tag{51}$$

where B_n is a vector of amplitude coefficients, which we obtain up to a scalar constant, and $\boldsymbol{\beta}$ is the Bloch vector, which must be chosen so that the boundary condition is satisfied. To this end, we will consider the cylinder centred at the origin, since boundary conditions elsewhere follow from quasiperiodicity. From the perspective of this cylinder, the incoming field, which includes radiation from other cylinders, is given by

$$u_0^i(\mathbf{r}) = \sum_{n=-\infty}^{\infty} B_n \sum_{p=-\infty}^{\infty} {\sum_{j=-\infty}^{\infty}}' e^{i\mathbf{R}_{jp}\cdot\boldsymbol{\beta}} \mathcal{H}_n(\mathbf{r} - \mathbf{R}_{jp}), \tag{52}$$

where the prime indicates that the term with $\mathbf{R}_{jp} = 0$ is to be omitted. We can use Graf's Addition Theorem [11]

$$\mathcal{H}_n(\mathbf{r}_{jp}) = \sum_{m=-\infty}^{\infty} \mathcal{H}_{n-m}(-\mathbf{R}_{j,p-q}) \mathcal{J}_m(\mathbf{r}_{0q}), \tag{53}$$

to expand the incoming field about the cylinder centred at r_{0q}. Interchanging the indices m and n gives us

$$u_0^i(\mathbf{r}) = \sum_{m=-\infty}^{\infty} B_m \sum_{p=-\infty}^{\infty} {\sum_{j=-\infty}^{\infty}}' e^{i\mathbf{R}_{jp}\cdot\boldsymbol{\beta}} \sum_{n=-\infty}^{\infty} \mathcal{H}_{m-n}(-\mathbf{R}_{jp}) \mathcal{J}_n(\boldsymbol{r}). \tag{54}$$

The scattered response is given by

$$u_0^s(\mathbf{r}) = \sum_{n=-\infty}^{\infty} B_n \mathcal{H}_n(\mathbf{r}), \tag{55}$$

thus, evaluating the total field $u_0(\mathbf{r}) = u_0^i(\mathbf{r}) + u_0^s(\mathbf{r})$ at the origin and applying the boundary condition gives us the dispersion relation for Bloch waves

$$1 + Z_n \sum_{m=-\infty}^{\infty} \frac{B_m}{B_n} \tau_{m-n}(\boldsymbol{\beta}) = 0 \tag{56}$$

where

$$\tau_n(\boldsymbol{\beta}) = G_n^{(-\infty,-1)}(\mathbf{0}, \boldsymbol{\beta}) + \sigma_{-n}(\boldsymbol{\beta}) + G_n^{(1,\infty)}(\mathbf{0}, \boldsymbol{\beta}), \tag{57}$$

and

$$Z_n = \frac{J_n(ka)}{H_n^{(1)}(ka)} \tag{58}$$

for Dirichlet boundary conditions, and

$$Z_n = \frac{J_n'(ka)}{H_n'^{(1)}(ka)} \tag{59}$$

for Neumann boundary conditions. Given fixed values for all other parameters, (56) must be solved for β_y, and for B_n (up to a multiplicative constant). Now, Bloch waves exist in pairs propagating in opposite directions. Since we will be studying excitation of Bloch waves at $y = 0$, then for each pair of Bloch waves found, only one will propagate in the positive y direction. This means that there will be, say, $2n$ solutions for β_y, and of these, only n will correspond to Bloch waves transporting energy into the lattice. To identify these, we evaluate (31) for each solution, and if $\langle E_S \rangle < 0$, we can discard the corresponding β_y value.

To determine the range for β_y, let us introduce the reciprocal lattice vectors

$$\mathbf{s}_1^* = \frac{2\pi}{s_1} \left[1, -\frac{\eta_1}{\eta_2}\right], \qquad \mathbf{s}_2^* = \frac{2\pi}{\eta_2} [0, 1] \tag{60}$$

such that $\mathbf{s}_j \cdot \mathbf{s}_p^* = 2\pi\delta_{jp}$, where δ_{jp} is the Kronecker delta, i.e.

$$\delta_{jp} = \begin{cases} 0, & j \neq p \\ 2\pi, & j = p. \end{cases} \tag{61}$$

Thus, if

$$\mathbf{R}_{mn}^* = (m\mathbf{s}_1^* + n\mathbf{s}_n^*), \qquad m, n \in \mathbb{Z}, \tag{62}$$

then

$$e^{i\mathbf{R}_{jp}\cdot(\boldsymbol{\beta}+\mathbf{R}_{mn}^*)} = e^{i\mathbf{R}_{jp}\cdot\boldsymbol{\beta}} \tag{63}$$

for any combination of integers j, p, m, and n. All possibilities are therefore accounted for if we consider

$$0 \leq \beta_y < 2\pi/\eta_2. \tag{64}$$

Now, (51) satisfies the quasiperiodicity property (9), and hence we can express it in the form (28) for some amplitude coefficients $c_j^{\pm}$. In terms of quasiperiodic Green's functions, we have

$$u^b(\mathbf{r}) = \sum_{n=-\infty}^{\infty} B_n \left[G_n^{(q_0,\infty)}(\mathbf{r}, \boldsymbol{\beta}) + G_n^{(-\infty,q_1)}(\mathbf{r}, \boldsymbol{\beta}) \right] \tag{65}$$

with $q_0 = 1 + q_1$, and so, upon using (46) and (47), we can read off

$$c_j^+ = \sum_{n=-\infty}^{\infty} \frac{2B_n(-i)^{n+1}}{s_1} \frac{e^{q_1 w_j^+}}{\gamma(\beta_{xj})(1 - e^{-w_j^+})} \left[\frac{k}{\beta_{xj} + \gamma(\beta_{xj})} \right]^n, \tag{66}$$

and

$$c_j^- = \sum_{n=-\infty}^{\infty} \frac{2B_n(-i)^{n+1}}{s_1} \frac{e^{(1+q_1)w_j^-}}{\gamma(\beta_{xj})(1 - e^{w_j^-})} \left[\frac{k}{\beta_{xj} - \gamma(\beta_{xj})} \right]^n. \tag{67}$$

3.2 Excitation Problem

We will now consider the interaction of a plane wave propagating at an angle ψ_0 to the edge of a semi-infinite lattice. Such a wave takes the form

$$u^i(\mathbf{r}) = e^{ik(x\cos\psi_0 + y\sin\psi_0)}. \tag{68}$$

This can be expanded as a series of nonsingular wave functions about the point $\mathbf{r} = \mathbf{R}_{jq}$ [19]; thus

$$u^i(\mathbf{r}) = e^{iq\mathbf{s_2}\cdot\mathbf{k}} \sum_{n=-\infty}^{\infty} i^n e^{-in\psi_0} \mathcal{J}_n(\mathbf{r}_{0q}) \tag{69}$$

and the scattered response takes the form

$$u^s(\mathbf{r}) = \sum_{n=-\infty}^{\infty} \sum_{p=0}^{\infty}{}' \sum_{j=-\infty}^{\infty}{}' A_n^p e^{ijks_1 \cos\psi_0} \mathcal{H}_n(\mathbf{r}_{jp}) \tag{70}$$

for some amplitude coefficient A_n^q.

We can now apply Graf's addition theorem (53). Terms with $j = 0$ and $p = q$ therefore do not need re-expanding, and so, separating out these terms , we find that

$$u^s(\mathbf{r}) = \sum_{n=-\infty}^{\infty} \left[A_n^q \mathcal{H}(\mathbf{r}_{0q}) + \sum_{p=0}^{\infty} \sum_{j=-\infty}^{\infty}{}' A_n^p e^{ijks_1 \cos\psi_0} \mathcal{H}_n(\mathbf{r}_{jp}) \right], \tag{71}$$

where the primes indicate that terms with $j = 0$ and $p = q$ are to be omitted. Applying (53) gives us

$$u^s(\mathbf{r}) = \sum_{n=-\infty}^{\infty} \left[A_n^q \mathcal{H}(\mathbf{r}_{0q}) + \sum_{p=0}^{\infty} \sum_{j=-\infty}^{\infty}{}' A_n^p e^{ijks_1 \cos\psi_0} \sum_{m=-\infty}^{\infty} \mathcal{H}_{n-m}(-\mathbf{R}_{j,p-q}) \mathcal{J}_m(\mathbf{r}_{0q}) \right]. \tag{72}$$

Combining this with (69), we obtain the total field

$$u(\mathbf{r}) = \sum_{n=-\infty}^{\infty} \Bigg[A_n^q \mathcal{H}(\mathbf{r}_{0q}) + e^{i(q\mathbf{s_2}\cdot\mathbf{k} - n\psi_0)} i^n \mathcal{J}_n(\mathbf{r}_{oq}) \tag{73}$$

$$+ \sum_{p=0}^{\infty} \sum_{j=-\infty}^{\infty}{}' A_n^p e^{ijks_1 \cos\psi_0} \sum_{m=-\infty}^{\infty} \mathcal{H}_{n-m}(-\mathbf{R}_{j,p-q}) \mathcal{J}_m(\mathbf{r}_{0q}) \Bigg], \tag{74}$$

where the terms involving $\mathcal{J}_n$ represent the field incident on the cylinder centred at r_{0q}, including the incident plane wave and the scattered response from other cylinders, and the terms involving $\mathcal{H}_n$ represent the scattered response. Thus, if we write

$$u(\mathbf{r}) = \sum_{n=-\infty}^{\infty} \left[A_n^q \mathcal{H}_n(\mathbf{r}_{0q}) + I_n^q \mathcal{J}_n(\mathbf{r}_{0q}) \right], \tag{75}$$

we see that

$$I_n^q = i^n e^{i(q\mathbf{s_2}\cdot\mathbf{k}-n\psi_0)} + \sum_{m=-\infty}^{\infty}\sum_{p=0}^{\infty}\sum_{j=-\infty}^{\infty}{}' A_m^p e^{ijks_1\cos\psi_0}\mathcal{H}_{m-n}(-\mathbf{R}_{j,p-q}), \tag{76}$$

or, after separating the term with $p = q$, we have

$$I_n^q = i^n e^{i(q\mathbf{s_2}\cdot\mathbf{k}-n\psi_0)} + \sum_{m=-\infty}^{\infty}\sum_{p=0}^{\infty} A_m^p S_{m-n}^{q-p}(k\cos\psi_0), \tag{77}$$

where

$$S_n^p = \begin{cases} \sigma_{-n}(k\cos\psi_0) & \text{if} \quad p = 0 \\ G_n(p\mathbf{s_2}, k\cos\psi_0) & \text{otherwise.} \end{cases} \tag{78}$$

Applying the Dirichlet boundary condition (9) at $\mathbf{r}_{0q} = a$ to (75) and using orthogonality gives

$$0 = A_n^q H_n^{(1)}(ka) + I_n^q J_n(ka), \tag{79}$$

or

$$A_n^q + Z_n I_n^q = 0. \tag{80}$$

Hence, after using this to eliminate I_n^q, (77) can be written as

$$A_n^q + Z_n \sum_{m=-\infty}^{\infty}\sum_{p=0}^{\infty} A_m^p S_{m-n}^{q-p}(k\cos\psi_0) = T_n^q, \qquad n \in \mathbb{Z},\ q = 0, 1, \ldots, \tag{81}$$

where

$$T_n^q = -Z_n i^n e^{i(q\mathbf{s_2}\cdot\mathbf{k}-n\psi_0)}. \tag{82}$$

3.3 Filtering Method

Now, if Bloch waves are present, the system (81) is non-convergent because of the non-decaying property of Bloch waves, hence $A_n^q \not\to 0$ as $q \to \infty$ and we

cannot simply solve by truncation. To compute A_n^q, we therefore decompose it into decaying and non-decaying parts, i.e.

$$A_n^q = \hat{A}_n^q + \sum_{\mu=1}^{\lambda} B_n^{(\mu)} e^{iq\mathbf{s}_2\cdot\boldsymbol{\beta}^{(\mu)}}, \tag{83}$$

where, having found λ Bloch waves, $B_n^{(\mu)}$ are the amplitude coefficients. $\hat{A}_n^q$ is therefore the decaying part of the amplitude coefficients, so that $\hat{A}_n^q \to 0$ as $q \to \infty$. Thus, if we eliminate the non-decaying part of A_n^q, we can obtain a convergent system that is straightforward to solve numerically. To this end, we introduce the "filtered coefficient" discussed in Section 4.2 for point-scatterers and 5.1 for finite-sized scatterers. The results obtained in Section 4.5 demonstrate the accuracy of this method, before we move on to obtain results for finite-sized scatterers.

4 Point Scatterers

The point-scatterer problem only requires the leading order terms in the expansions of the Green's functions discussed in Section 2.4, hence we omit the sum over n use the Green's functions of order zero. Hence, for the propagation problem, a Bloch wave takes the form

$$u^b(\mathbf{r}) = BG_0^{(-\infty,\infty)}(\mathbf{r}, \boldsymbol{\beta}). \tag{84}$$

From the perspective of the cylinder centred at the origin, the incoming and scattered fields, respectively, are given by

$$u_0^i(\mathbf{r}) = B \sum_{p=-\infty}^{\infty} {\sum_{j=-\infty}^{\infty}}' e^{i\mathbf{R}_{jp}\cdot\boldsymbol{\beta}} H_0^{(1)}(k|\mathbf{r} - \mathbf{R}_{jp}|), \tag{85}$$

and

$$u_0^s(\mathbf{r}) = BH_0^{(1)}(kr), \tag{86}$$

where the prime indicates that terms with $\mathbf{R}_{jp} = 0$ are to be omitted. The total field, obtained after using Graf's addition theorem on the incoming field, takes the form

$$u_0(\mathbf{r}) = \sum_{j=-\infty}^{\infty} \sum_{p=-\infty}^{\infty} e^{i\mathbf{R}_{jp}\cdot\beta} H_0^{(1)}(kR_{jp}) J_0(kr) + H_0^{(1)}(kr). \tag{87}$$

Finally, we apply the boundary condition, and hence obtain our dispersion relation

$$1 + Z_0\tau_0 = 0. \tag{88}$$

This can be simplified by observing that $\Re[\tau_0] = -1$ as in [9], so that we have

$$1 + Z_0(-1 + i\Im[\tau_0]) = 0, \tag{89}$$

or

$$(1 - Z_0) + iZ_0\Im[\tau_0] = 0. \tag{90}$$

Thus, the dispersion relation can be written as

$$1 + W_0\Im[\tau_0(\boldsymbol{\beta})] = 0, \tag{91}$$

where

$$W_0 = iZ_0/(1 - Z_0) = J_0(ka)/Y_0(ka), \tag{92}$$

which is real. Using the expansions of the semi-infinite Green's functions with $q_1 = q$ and $q_0 = 1 + q$, we can expand (84) in the form (28), with

$$c_j^+ = \frac{2Bie^{qw_j^+}}{s_1\gamma(\beta_{xj})(e^{-w_j^+} - 1)} \tag{93}$$

and

$$c_j^- = \frac{2B_nie^{(1+q)w_j^-}}{s_1\gamma(\beta_{xj})(e^{w_j^-} - 1)}. \tag{94}$$

For the purpose of evaluating (31), we have

$$|c_j^+|^2 = \frac{4|B|^2}{s_1^2|\gamma(\beta_{xj})e^{-w_j^+} - 1|^2}, \qquad |c_j^-|^2 = \frac{4|B|^2}{s_1^2|\gamma(\beta_{xj})e^{w_j^-} - 1|^2}, \quad j \in \mathcal{M}. \tag{95}$$

and

$$\Im[c_j^+(c_j^-)^*] = \left|\frac{B}{s_1\gamma(\beta_{xj})}\right|^2 \Im[\mathrm{csch}^2(w_j^+/2)]. \tag{96}$$

4.1 Excitation Problem

Consider a plane wave incident on a semi-infinite lattice of small cylinders as in Section 3.2. The scattered response is given by

$$u^s(\mathbf{r}) = \sum_{p=0}^{\infty} A_p \sum_{j=-\infty}^{\infty} e^{ijs_1 k\cos\psi_0} H_0^{(1)}(k|\mathbf{r}-\mathbf{R}_{jp}|). \tag{97}$$

The incoming and scattered fields from the perspective of the cylinder located at $\mathbf{R}_{0q}$, respectively, are:

$$u_0^i(\mathbf{r}) = e^{ik(x\cos\psi_0 + y\sin\psi_0)} + \sum_{p=0}^{\infty} A_p \sum_{j=-\infty}^{\infty}{}' e^{ijs_1 k\cos\psi_0} H_0^{(1)}(k|\mathbf{r}-\mathbf{R}_{jp}|), \tag{98}$$

where the prime indicates that the term with $j = 0$ and $p = q$ is to be omitted, and

$$u_0^s(\mathbf{r}) = A_q H_0^{(1)}(k|\mathbf{r}-\mathbf{R}_{0q}|). \tag{99}$$

Using Graf's Addition Theorem on the incoming field, and applying the Dirichlet boundary condition to the total field $u = u^i + u^s$ on the cylinder centred at $\mathbf{R}_{0q}$ (boundary conditions at other cylinders follow from quasiperiodicity) leads to

$$A_q + Z_0 \sum_{p=0}^{\infty} A_p S_{q-p} = T_q, \qquad q = 0, 1, \ldots, \tag{100}$$

where

$$T_q = -Z_0 e^{iqk(\eta_1\cos\psi_0 + \eta_2\sin\psi_0)}. \tag{101}$$

Note that (100) can be obtained by setting $m = n = 0$ in (81).

4.2 Filtering Equations

If a single Bloch wave is excited, we have

$$A_q = Be^{iq\mathbf{s}_2\cdot\boldsymbol{\beta}} + \hat{A}_q. \tag{102}$$

This decomposition yields a further unknown coefficient B, which we can "filter out" by introducing the filtered coefficient $A_q^{(1)}$ such that

$$A_q^{(1)} = \begin{cases} A_0 & \text{if } q = 0, \\ A_q - e^{i\mathbf{s}_2\cdot\boldsymbol{\beta}} A_{q-1} & \text{otherwise.} \end{cases} \tag{103}$$

The aim now is to construct and solve a system of equations for $A_q^{(1)}$, which can then be used to reconstruct the original coefficients A_q. To this end, we solve the recurrence relation (103) for A_q, giving us

$$A_q = \sum_{j=0}^{q} A_j^{(1)} e^{i(q-j)\mathbf{s}_2\cdot\boldsymbol{\beta}}. \tag{104}$$

Now, there are two ways we could obtain our filtered system. The approach used in [10] involves taking phase shifted differences between consecutive equations in (100). This poses the problem of the special case where $q = 0$, since there is no preceding equation. If two Bloch waves are excited, then the equations with $q = 0$ and $q = 1$ both require special treatment, and so on, meaning that this approach is difficult to generalise for an arbitrary number of Bloch waves. Instead, we substitute (104) into the system (100) to obtain

$$\sum_{j=0}^{q} A_j^{(1)} e^{i(q-j)\mathbf{s}_2\cdot\boldsymbol{\beta}} + Z_0 \sum_{p=0}^{\infty} \sum_{j=0}^{p} A_j^{(1)} e^{i(p-j)\mathbf{s}_2\cdot\boldsymbol{\beta}} S_{q-p} = T_q. \tag{105}$$

This cannot be solved by truncation, since the inner sum contains $A_0^{(1)}$, $A_1^{(1)}, \ldots$ for every p. However, if we interchange the summations over j and p, i.e.

$$\sum_{j=0}^{q} A_j^{(1)} e^{i(q-j)\mathbf{s}_2\cdot\boldsymbol{\beta}} + Z_0 \sum_{j=0}^{\infty} A_j^{(1)} \sum_{p=j}^{\infty} e^{i(p-j)\mathbf{s}_2\cdot\boldsymbol{\beta}} S_{q-p} = T_q, \tag{106}$$

and sum the result over p, we now have a convergent system

$$\sum_{j=0}^{q} A_j^{(1)} e^{i(q-j)\mathbf{s}_2\cdot\boldsymbol{\beta}} + Z_0 \sum_{j=0}^{\infty} A_j^{(1)} e^{i(q-j)\mathbf{s}_2\cdot\boldsymbol{\beta}} \Gamma_{j-q}(\boldsymbol{\beta}) = T_q, \tag{107}$$

where

$$\Gamma_j(\boldsymbol{\beta}) = \begin{cases} G_0^{(j,\infty)}(\mathbf{0},\boldsymbol{\beta}) & \text{if} \quad j > 0 \\ G_0^{(1,\infty)}(\mathbf{0},\boldsymbol{\beta}) + \sigma_0(k\cos\psi_0) & \text{if} \quad j = 0 \\ G_0^{(j,-1)}(\mathbf{0},\boldsymbol{\beta}) + G_0^{(1,\infty)}(\mathbf{0},\boldsymbol{\beta}) + \sigma_0(k\cos\psi_0) & \text{if} \quad j < 0. \end{cases} \tag{108}$$

The same method can be used for multiple Bloch waves by using the decomposition

$$A_q = \hat{A}_q + \sum_{m=1}^{\lambda} B^{(m)} e^{iq\mathbf{s}_2\cdot\boldsymbol{\beta}^{(m)}} \tag{109}$$

and introducing the filtered coefficient $A_q^{(\lambda)}$ such that

$$A_q^{(\lambda)} = \begin{cases} A_q & \text{if } q = 0 \text{ or } \lambda = 0 \\ A_q^{(\lambda-1)} - e^{i\mathbf{s}_2\cdot\boldsymbol{\beta}^{(\lambda)}} A_{q-1}^{(\lambda-1)} & \text{otherwise} \end{cases} \tag{110}$$

where $A_q^{(0)}$ is the unfiltered coefficient and $A_q^{(\lambda)}$ has the first λ Bloch waves filtered out. We proceed as for the single Bloch wave case by solving the recurrence relation (110) for

$$A_q^{(\lambda-1)} = \sum_{j=0}^{q} A_j^{(\lambda)} e^{i(q-j)\mathbf{s}_2\cdot\boldsymbol{\beta}^{(\lambda)}}, \tag{111}$$

however we require an expression for $A_q^{(0)}$ in terms of $A_j^{(\lambda)}$ in order to reconstruct our original coefficients. Applying (111) to $A_q^{(0)}$ twice gives us

$$A_q^{(0)} = \sum_{j=0}^{q} A_j^{(1)} e^{i(q-j)\mathbf{s}_2\cdot\boldsymbol{\beta}^{(1)}} \tag{112}$$

$$= \sum_{j=0}^{q}\sum_{p=0}^{j} A_p^{(2)} e^{i(j-p)\mathbf{s}_2\cdot\boldsymbol{\beta}^{(2)}} e^{i(q-j)\mathbf{s}_2\cdot\boldsymbol{\beta}^{(1)}} \tag{113}$$

$$= d_{2,1}\sum_{p=0}^{q} A_p^{(2)} e^{i(q-p)\mathbf{s}_2\cdot\boldsymbol{\beta}^{(1)}} + d_{1,2}\sum_{p=0}^{q} A_p^{(2)} e^{i(q-p)\mathbf{s}_2\cdot\boldsymbol{\beta}^{(2)}}, \tag{114}$$

where

$$d_{n,m} = \frac{1}{1 - e^{i\mathbf{s}_2\cdot(\boldsymbol{\beta}^{(n)} - \boldsymbol{\beta}^{(m)})}}. \tag{115}$$

Repeating this process, we obtain

$$A_q^{(0)} = d_{2,1}\sum_{p=0}^{q}\sum_{j=0}^{p} A_j^{(3)} e^{i(p-j)\mathbf{s_2}\cdot\boldsymbol{\beta}^{(3)}} e^{i(q-p)\mathbf{s_2}\cdot\boldsymbol{\beta}^{(1)}} + d_{1,2}\sum_{p=0}^{q}\sum_{j=0}^{p} A_j^{(3)} e^{i(p-j)\mathbf{s_2}\cdot\boldsymbol{\beta}^{(3)}} e^{i(q-p)\mathbf{s_2}\cdot\boldsymbol{\beta}^{(2)}} \tag{116}$$

$$= d_{2,1}d_{3,1}\sum_{j=0}^{q} A_j^{(3)} e^{i(q-j)\mathbf{s_2}\cdot\boldsymbol{\beta}^{(1)}} + d_{1,2}d_{3,2}\sum_{j=0}^{q} A_j^{(3)} e^{i(q-j)\mathbf{s_2}\cdot\boldsymbol{\beta}^{(2)}} + d_{1,3}d_{2,3}\sum_{j=0}^{q} A_j^{(3)} e^{i(q-j)\mathbf{s_2}\cdot\boldsymbol{\beta}^{(3)}}, \tag{117}$$

since

$$d_{2,1}d_{1,3} + d_{1,2}d_{2,3} = d_{1,3}d_{2,3}. \tag{118}$$

Hence, for the cases where $\lambda = 1, 2, 3$, we have

$$A_q^{(0)} = \sum_{m=1}^{\lambda} Q_m^{\lambda} \sum_{j=0}^{q} A_j^{(\lambda)} e^{i(q-j)\mathbf{s}_2\cdot\boldsymbol{\beta}^{(m)}}, \tag{119}$$

where

$$Q_1^1 = 1, \qquad Q_m^{\lambda} = \prod_{n=1}^{\lambda} d_{n,m}, \quad n \neq m. \tag{120}$$

To show that (119) is true for all $\lambda \in \mathbb{N}$, we start by using (111) to obtain

$$\begin{aligned} A_q^{(0)} &= \sum_{m=1}^{\lambda} Q_m^{\lambda} \sum_{j=0}^{q}\sum_{p=0}^{j} A_p^{(\lambda+1)} e^{i(j-p)\mathbf{s}_2\cdot\boldsymbol{\beta}^{(\lambda+1)}} e^{i(q-j)\mathbf{s}_2\cdot\boldsymbol{\beta}^{(m)}} \\ &= \sum_{m=1}^{\lambda} Q_m^{\lambda} e^{iq\mathbf{s}_2\cdot\boldsymbol{\beta}^{(m)}} \sum_{p=0}^{q} A_p^{(\lambda+1)} e^{-ip\mathbf{s}_2\cdot\boldsymbol{\beta}^{(\lambda+1)}} \sum_{j=p}^{q} e^{ij\mathbf{s}_2\cdot(\boldsymbol{\beta}^{(\lambda+1)}-\boldsymbol{\beta}^{(m)})} \\ &= \sum_{m=1}^{\lambda} Q_m^{\lambda} d_{\lambda+1,m} \sum_{p=0}^{q} A_p^{(\lambda+1)} e^{i(q-p)\mathbf{s}_2\cdot\boldsymbol{\beta}^{(m)}} + \sum_{m=1}^{\lambda} Q_m^{\lambda} d_{m,\lambda+1} \sum_{p=0}^{q} A_p^{(\lambda+1)} e^{i(q-p)\mathbf{s}_2\cdot\boldsymbol{\beta}^{(\lambda+1)}} \\ &= \sum_{m=1}^{\lambda} Q_m^{\lambda+1} \sum_{p=0}^{q} A_p^{(\lambda+1)} e^{i(q-p)\mathbf{s}_2\cdot\boldsymbol{\beta}^{(m)}} + \sum_{m=1}^{\lambda} Q_m^{\lambda} d_{m,\lambda+1} \sum_{p=0}^{q} A_p^{(\lambda+1)} e^{i(q-p)\mathbf{s}_2\cdot\boldsymbol{\beta}^{(\lambda+1)}}. \end{aligned} \tag{121}$$

Hence, if we can show that

$$\sum_{m=1}^{\lambda} Q_m^{\lambda} d_{m,\lambda+1} = Q_{\lambda+1}^{\lambda+1}, \tag{122}$$

then (119) is established for all $\lambda > 1$. Now, if $\lambda > 1$, then (122) is equivalent to

$$\sum_{m=1}^{\lambda} \prod_{n=1}^{\lambda} \frac{d_{n,m}}{d_{n,\lambda+1}} = 1, \qquad n \neq m, \tag{123}$$

and so, setting $z_m = e^{-\mathbf{s}_2 \cdot \boldsymbol{\beta}^{(m)}}$, the proof follows from applying the result in the appendix.

As in the case of one Bloch wave, we substitute (119) into (100) and interchange summations to obtain our convergent system

$$\sum_{m=1}^{\lambda} Q_m^{\lambda} \left[\sum_{j=0}^{q} A_j^{(\lambda)} e^{i(q-j)\mathbf{s}_2 \cdot \boldsymbol{\beta}^{(m)}} + Z_0 \sum_{j=0}^{\infty} A_j^{(\lambda)} e^{i(q-j)\mathbf{s}_2 \cdot \boldsymbol{\beta}^{(m)}} \Gamma_{j-q}(\beta^{(m)}) \right] = T_q, \quad q = 0, 1, \ldots. \tag{124}$$

Next, having solved (124) for $A_j^{(\lambda)}$, we substitute this into (119) to obtain $A_q^{(0)}$ and, using (110), therefore compute A_q for arbitrarily large q. For large enough q, say q_{inf}, $\hat{A}_q$ becomes negligible and we have from (109)

$$A_{q_{\text{inf}}} \approx \sum_{m=1}^{\lambda} B^{(m)} e^{iq_{\text{inf}}\mathbf{s}_2 \cdot \boldsymbol{\beta}^{(m)}}. \tag{125}$$

Furthermore, using the fact that $A_q^{(0)} = A_q$, (119) can be written as

$$A_{q_{\text{inf}}} = \sum_{m=1}^{\lambda} Q_m^{\lambda} \sum_{j=0}^{q_{\text{inf}}} A_j^{(\lambda)} e^{i(q_{\text{inf}}-j)\mathbf{s}_2 \cdot \boldsymbol{\beta}^{(m)}}. \tag{126}$$

Equating (126) and (125), we obtain an expression for the Bloch coefficients, i.e.

$$B^{(m)} = Q_m^{\lambda} \sum_{j=0}^{q_{\text{inf}}} A_j^{(\lambda)} e^{-ij\mathbf{s}_2 \cdot \boldsymbol{\beta}^{(m)}}. \tag{127}$$

4.3 Infinite Array Subtraction

Having computed the Bloch vector $\boldsymbol{\beta}^{(m)}$ and corresponding Bloch amplitude coefficients $B^{(m)}$, we can now generate a convergent system of equations for $\hat{A}_q$ by substituting (109) into (100) and moving the terms involving Bloch waves to the

right-hand side. Note that the system will only converge for the correct values of $\boldsymbol{\beta}^{(m)}$ and $B^{(m)}$, and so this provides us with a useful tool to test our results.

We find that

$$\hat{A}_q + Z_0 \sum_{p=0}^{\infty} \hat{A}_p S_{q-p} = T_q - \sum_{m=1}^{\lambda} B^{(m)} e^{iq\mathbf{s}_2\cdot\boldsymbol{\beta}^{(m)}} - Z_0 \sum_{p=0}^{\infty} B^{(m)} e^{ip\mathbf{s}_2\cdot\boldsymbol{\beta}^{(m)}} S_{q-p} \quad (128)$$

$$= T_q - \sum_{m=1}^{\lambda} B^{(m)} e^{iq\mathbf{s}_2\cdot\boldsymbol{\beta}^{(m)}} \left[1 + Z_0 \sum_{p=-q}^{\infty} e^{ip\mathbf{s}_2\cdot\boldsymbol{\beta}^{(m)}} S_{-p}\right]. \quad (129)$$

This can be simplified using the definition (78) of S_{-p} ,

$$\sum_{p=-q}^{\infty} e^{ip\mathbf{s}_2\cdot\boldsymbol{\beta}^{(m)}} S_{-p} = G_0^{(-q,-1)}(0,\boldsymbol{\beta}^{(m)}) + \sigma_0(\beta_x) + G_0^{(1,\infty)}(0,\boldsymbol{\beta}^{(m)}) \quad (130)$$

$$= \tau_0(\beta_x) - G_0^{(-\infty,-q-1)}(0,\boldsymbol{\beta}^{(m)}), \quad (131)$$

and utilising the dispersion relationship (88). Hence, we obtain

$$\hat{A}_q + Z_0 \sum_{p=0}^{\infty} \hat{A}_p S_{q-p} = T_q + Z_0 \sum_{m=1}^{\lambda} B^{(m)} e^{iq\mathbf{s}_2\cdot\boldsymbol{\beta}^{(m)}} G_0^{(-\infty,-q-1)}(0,\boldsymbol{\beta}^{(m)}). \quad (132)$$

4.4 Reflection and Transmission

To calculate the reflection and transmission coefficients, we require the spectral forms of the Green's function (44) of order zero for semi-infinite lattices, given by [18]

$$G_0^{(q_0,\infty)}(\mathbf{r},\boldsymbol{\beta}) = \frac{2i}{s_1} \sum_{j=-\infty}^{\infty} e^{q_0 w_j^-} \frac{e^{i\beta_{xj}x+\gamma(\beta_{xj}y)}}{\gamma(\beta_{xj})(e^{w_j^-}-1)}, \quad y \le q_0\eta_2, \quad (133)$$

and

$$G_0^{(-\infty,q1)}(\mathbf{r},\boldsymbol{\beta}) = \frac{2i}{s_1} \sum_{j=-\infty}^{\infty} e^{q_1 w_j^+} \frac{e^{i\beta_{xj}x-\gamma(\beta_{xj}y)}}{\gamma(\beta_{xj})(e^{-w_j^+}-1)}, \quad y \ge q_1\eta_2, \quad (134)$$

where $w_j^{\pm} = \pm\eta_2\gamma(\beta_{xj}) + i(\eta_2\beta_y - 2j\pi\eta_1/s_1)$. For a row of sources centred at $\mathbf{r} = \mathbf{R}_{j0}$, we have

$$G_0(\mathbf{r},\boldsymbol{\beta}) = -\frac{2i}{s_1} \sum_{j=-\infty}^{\infty} \frac{e^{i\beta_{xj}x}}{\gamma(\beta_{xj})} e^{-\gamma(\beta_{xj})|y|}. \quad (135)$$

Now, in terms of scattering angles ψ_j, we have $\beta_{xj} = k\cos\psi_j$, where

$$\cos\psi_j = k\cos\psi_0 + 2j\pi/s_1 \qquad \text{and} \qquad \sin\psi_j = i\gamma(k\cos\psi_j), \tag{136}$$

so that between two consecutive rows, the total field may be written as

$$u(\mathbf{r}) = \sum_{j=-\infty}^{\infty} e^{ikx\cos\psi_j}[c_{jq}^{-}e^{-iky\sin\psi_j} + c_{jq}^{+}e^{iky\sin\psi_j}], \quad (q-1)\eta_2 \le y \le q\eta_2. \tag{137}$$

For later purposes, let us define

$$\tau_j = e^{ik(\eta_1\cos\psi_j - \eta_2\sin\psi_j)} \qquad \text{and} \qquad \rho_j = e^{-ik(\eta_1\cos\psi_j + \eta_2\sin\psi_j)}, \tag{138}$$

giving us

$$e^{w_j^{+}} = \rho_j e^{i\mathbf{s}_2\cdot\boldsymbol{\beta}}, \qquad e^{w_j^{-}} = \tau_j^{-1}e^{i\mathbf{s}_2\cdot\boldsymbol{\beta}}. \tag{139}$$

Below the lattice, where the only upward propagating mode is the incident field, we have

$$u(\mathbf{r}) = \sum_{j=-\infty}^{\infty} e^{ikx\cos\psi_j}[c_{j0}^{-}e^{-iky\sin\psi_j} + \delta_{j0}e^{iky\sin\psi_j}], \quad y \le 0. \tag{140}$$

Writing the scattered field in terms of quasiperiodic Green's functions, i.e.

$$u^s(\mathbf{r}) = \sum_{m=1}^{\lambda} B^{(m)}G_0^{(0,\infty)}(\mathbf{r}, \boldsymbol{\beta}^{(m)}) + \sum_{p=0}^{\infty}\hat{A}_p G_0(\mathbf{r} - p\mathbf{s}_2), \tag{141}$$

and utilising the spectral forms of the Green's functions, we may read off the reflection coefficient as

$$c_{j0}^{-} = \frac{2}{ks_1\sin\psi_j}\left[\sum_{m=1}^{\lambda}\frac{B^{(m)}\tau_j}{\tau_j - e^{i\mathbf{s}_2\cdot\boldsymbol{\beta}^{(m)}}} + \sum_{p=0}^{\infty}\hat{A}_p\tau_j^{-p}\right]. \tag{142}$$

To calculate the transmitted field, we split the total field into decaying and non-decaying parts, i.e.

$$u(\mathbf{r}) = \hat{u}(\mathbf{r}) + u^b(\mathbf{r}) \tag{143}$$

where

$$\hat{u}(\mathbf{r}) = e^{ik(x\cos\psi_0 + y\sin\psi_0)} + \sum_{p=0}^{\infty} \hat{A}_p G_0(\mathbf{r} - p\mathbf{s}_2) - \sum_{m=1}^{\lambda} B^{(m)} G_0^{(-\infty,-1)}(\mathbf{r}, \boldsymbol{\beta}^{(m)}), \quad (144)$$

and

$$u^b(\mathbf{r}) = \sum_{m=1}^{\lambda} B^{(m)} G_0^{(-\infty,\infty)}(\mathbf{r}, \boldsymbol{\beta}^{(m)}) \quad (145)$$

is the non-decaying contribution from Bloch waves. We can now calculate the contributions to $c_j^{\pm}$ using the spectral forms of the Green's functions. Only the central term on the right-hand side of (176) includes downward propagating modes, and so we find that

$$\hat{c}_j^- = \frac{2}{ks_1 \sin\psi_j} \sum_{p=q}^{\infty} \hat{A}_p \tau_j^{-p}, \quad (146)$$

whereas all three terms on the right-hand side include upward propagating modes, and so we have

$$\hat{c}_j^+ = \delta_{j0} + \frac{2}{ks_1 \sin\psi_j} \left[\sum_{p=0}^{q-1} \hat{A}_p \rho_j^{-p} + \sum_{m=1}^{\lambda} \frac{B^{(m)}}{1 - \rho_j e^{i\mathbf{s}_2 \cdot \boldsymbol{\beta}^{(m)}}} \right]. \quad (147)$$

Finally, for the contributions from Bloch waves, we find that

$$c_{jq}^{b+} = \frac{2\rho_j^q}{ks_1 \sin\psi_j} \sum_{m=1}^{\lambda} \frac{B^{(m)} e^{i\mathbf{s}_2 \cdot \boldsymbol{\beta}^{(m)}}}{1 - \rho_j^{-1} e^{-i\mathbf{s}_2 \cdot \boldsymbol{\beta}^{(m)}}} \quad (148)$$

and

$$c_{jq}^{b-} = \frac{2\tau_j^{-q}}{ks_1 \sin\psi_j} \sum_{m=1}^{\lambda} \frac{B^{(m)} e^{i\mathbf{s}_2 \cdot \boldsymbol{\beta}^{(m)}}}{\tau_j e^{-i\mathbf{s}_2 \cdot \boldsymbol{\beta}^{(m)}} - 1}. \quad (149)$$

4.5 Results

In figure 2, we have the magnitudes of coefficients for a rectangular lattice with $s_1 = [1, 0]$, $s_2 = [0, 1]$ $a = 0.05$, and $\psi_0 = 0.25\pi$.

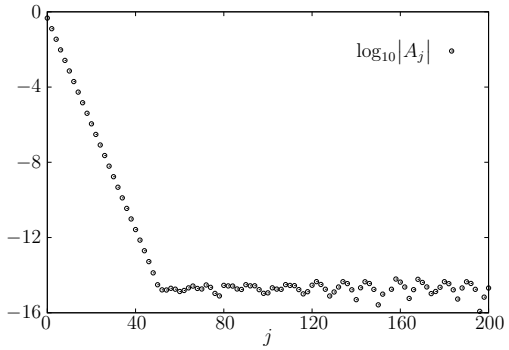

(a) $k = 1.5$

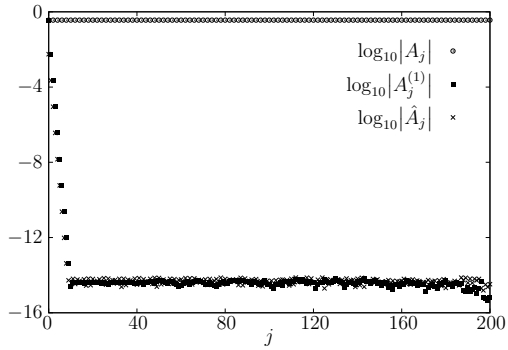

(b) k=3.0

Figure 2: Magnitudes of coefficients for a rectangular lattice with $s_1 = [1, 0]$, $s_2 = [0, 1]$, $a = 0.005$ and $\psi_0 = 0.25\pi$

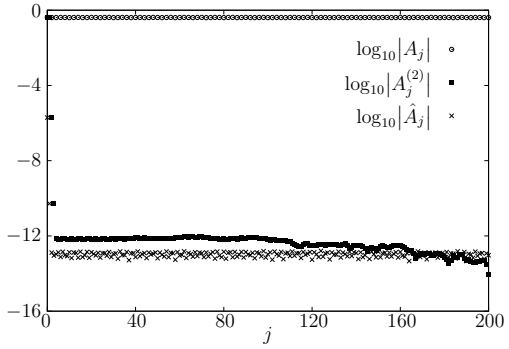

(a) $k = 3.7$, $\psi_0 = 0.15\pi$

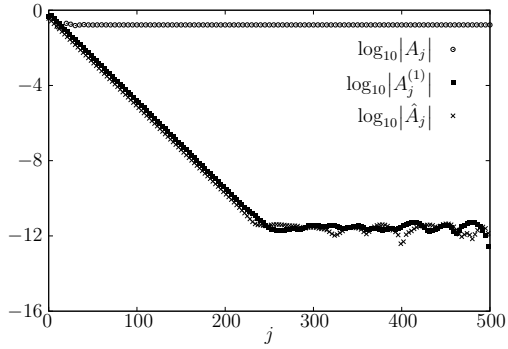

(b) $k = 3.525$, $\psi_0 = 0.16\pi$

Figure 3: Magnitudes of coefficients for a skewed lattice with $s_1 = [1, 0]$, $s_2 = [0.1, 1.2]$ and $a = 0.005$.

Figure 2(a) shows the magnitude of the amplitude coefficient A_j with $k = 1.5$. In this case, no Bloch waves are excited, and so this was calculated by solving (100), truncating the system at $p = 200$ and $q = 200$. We will use this result as a benchmark for testing the filtering method. Figure 2(b) shows that the magnitude of the filtered coefficient decay rapidly, so that they are negligible for $j > 45$. Computation of A_j using filtering and using infinite array subtraction are in agreement to 13-14 significant figures.

Note that, in the absence of Bloch waves, coefficients decay exponetially so that lines appear almost straight. In fact, the field inside the lattice is composed of damped modes, and if one of these damped modes moves near to the real axis, then decay is slower (as in figure 3(b)).

In figure 3, we have the magnitude coefficients for a skewed lattice, with $s_1 = [1, 0]$, $s_2 = [0.1, 1.2]$, $a = 0.005$. Figure 3(a) shows a case where two Bloch waves are excited, with $k = 3.7$ and $\psi_0 = 0.15\pi$. We see that the filtered coefficients and $\hat{A}_j$ decay rapidly, and results for A_j using infinite array subtraction are in agreement to 10 significant figures.

Figure 3(b) shows the case where $\psi_0 = 0.16\pi$ and $k = 3.525$, such that one Bloch wave is excited, but there would be a second Bloch wave if we increased the frequency slightly so that $k = 3.526$. We see that $A_j^{(1)}$ and $\hat{A}_j$ decay, but do so much slower than in typical cases. A_j computed using filtering is in agreement with A_j found using infinite array subtraction.

All of the numerical results obtained here satisfy the conservation of energy condition (190) discussed in Section 6. In the absence of Bloch waves, this condition is satisfied to near machine precision, whereas accuracy decreased to 12 significant figures in figure 3. This is to be expected due to increased computational complexity when Bloch waves are excited.

5 Finite Size Effects

Mathematically, the introduction of finite-size effects corresponds to increasing the number of terms retained in the expansions of the Green's functions up to order $|n| = N$, for some $N > 0$.

5.1 Filtering Equations

In the case where a single Bloch wave is excited, we have

$$A_n^q = B_n e^{iq\mathbf{s_2}\cdot\boldsymbol{\beta}} + \hat{A}_n^q, \tag{150}$$

where $\hat{A}_n^q \to 0$ as $q \to \infty$. To eliminate B_n from (81), we introduce the filtered coefficient

$$A_n^{q(1)} = \begin{cases} A_n^q & \text{if } q = 0, \\ A_n^q - e^{i\mathbf{s}_2\cdot\boldsymbol{\beta}} A_n^{q-1} & \text{otherwise} \end{cases} \tag{151}$$

and solve this to obtain

$$A_n^q = \sum_{j=0}^{q} A_n^{j(1)} e^{i(q-j)\mathbf{s}_2\cdot\boldsymbol{\beta}}. \tag{152}$$

Substituting this into (81) yields

$$\sum_{j=0}^{q} A_n^{j(1)} e^{i(q-j)\mathbf{s_2}\cdot\boldsymbol{\beta}} + Z_n \sum_{m=-\infty}^{\infty} \sum_{p=0}^{\infty} \sum_{j=0}^{p} A_m^{j(1)} e^{i(p-j)\mathbf{s}_2\cdot\boldsymbol{\beta}} S_{m-n}^{q-p} = T_n^q. \tag{153}$$

Finally, interchanging the summations over j and p leads to the convergent system

$$\sum_{j=0}^{q} A_n^{j(1)} e^{i(q-j)\mathbf{s_2}\cdot\boldsymbol{\beta}} + Z_n \sum_{m=-\infty}^{\infty} \sum_{j=0}^{\infty} A_m^{j(1)} e^{i(q-j)\mathbf{s}_2\cdot\boldsymbol{\beta}} \Gamma_{m-n}^{j-q} = T_n^q, \tag{154}$$

where

$$\Gamma_n^j(\boldsymbol{\beta}) = \begin{cases} G_n^{(j,\infty)}(\mathbf{0},\boldsymbol{\beta}) & \text{if} \quad j > 0 \\ G_n^{(1,\infty)}(\mathbf{0},\boldsymbol{\beta}) + \sigma_{-n}(k\cos\psi_0) & \text{if} \quad j = 0 \\ G_n^{(j,-1)}(\mathbf{0},\boldsymbol{\beta}) + G_n^{(1,\infty)}(\mathbf{0},\boldsymbol{\beta}) + \sigma_{-n}(k\cos\psi_0) & \text{if} \quad j < 0. \end{cases} \tag{155}$$

Similarly, for the case involving multiple Bloch waves, we have the decomposition (83) of A_n^q and we define the filtered coefficient

$$A_n^{q(\lambda)} = \begin{cases} A_n^q & \text{if } q = 0 \text{ or } \lambda = 0 \\ A_n^{q(\lambda-1)} - e^{i\mathbf{s_2}\cdot\boldsymbol{\beta}^{(\lambda)}} A_n^{(q-1)(\lambda-1)} & \text{otherwise,} \end{cases} \tag{156}$$

and solve this for

$$A_n^{q(0)} = \sum_{\mu=1}^{\lambda} Q_\mu^\lambda \sum_{j=0}^{q} A_n^{j(\lambda)} e^{i(q-j)\mathbf{s_2}\cdot\boldsymbol{\beta}^{(\mu)}}, \tag{157}$$

where $Q_\mu^{(\lambda)}$ is defined as (120)

Following the same procedure as before, we obtain our convergent system

$$\sum_{\mu=1}^{\lambda} Q_\mu^\lambda \left[\sum_{j=0}^{q} A_n^{j(\lambda)} e^{i(q-j)\mathbf{s_2}\cdot\boldsymbol{\beta}^{(\mu)}} + Z_n \sum_{m=-\infty}^{\infty} \sum_{j=0}^{\infty} A_m^{j(\lambda)} e^{i(q-j)\mathbf{s_2}\cdot\boldsymbol{\beta}^{(\mu)}} \Gamma_{m-n}^{j-q}(\boldsymbol{\beta}^{(\mu)}) \right] = T_n^q. \tag{158}$$

Now, using the fact that $A_n^{q(0)} = A_n^q$, we can equate the decomposition (83) with (157), choosing sufficiently large q, say q_{inf}, so that $\hat{A}_n^q$ are negligible, i.e.

$$\sum_{\mu=1}^{\lambda} Q_\mu^\lambda \sum_{j=0}^{q_{inf}} A_n^{j(\lambda)} e^{i(q_{inf}-j)\mathbf{s_2}\cdot\boldsymbol{\beta}} = \sum_{\mu=1}^{\lambda} B_n^{(\mu)} e^{iq_{inf}\mathbf{s_2}\cdot\boldsymbol{\beta^{(\mu)}}}. \tag{159}$$

After simplifications, the Bloch coefficients can be written explicitly as

$$B_n^{(\mu)} = Q_\mu^\lambda \sum_{j=0}^{q_{inf}} A_n^{j(\lambda)} e^{-ij\mathbf{s_2}\cdot\boldsymbol{\beta}^{(\mu)}}. \tag{160}$$

5.2 Infinite Array Subtraction

Consider the case where one Bloch wave is excited, so that the amplitude coefficients are given by $A_n^q = \hat{A}_n^q + B_n e^{iq\mathbf{s}_2\cdot\boldsymbol{\beta}}$, and the Bloch amplitude coefficients B_n are now known. Substituting this into (81) and moving terms involving Bloch waves to the right-hand side gives

$$\hat{A}_n^q + Z_n \sum_{m=-\infty}^{\infty}\sum_{p=0}^{\infty} \hat{A}_m^p S_{m-n}^{q-p}(k\cos\psi_0) = T_n^q - B_n e^{iq\mathbf{s}_2\cdot\boldsymbol{\beta}}\left[1 + Z_n \sum_{m=-\infty}^{\infty}\frac{B_m}{B_n}\sum_{p=-q}^{\infty} e^{ip\mathbf{s}_2\cdot\boldsymbol{\beta}} S_{m-n}^{-p}\right], \tag{161}$$

$n \in \mathbb{Z}$, $q = 0, 1, \ldots$. Using the definition of S_n^p, this can be simplified by writing

$$\sum_{p=-q}^{\infty} e^{ip\mathbf{s}_2\cdot\boldsymbol{\beta}} S_{m-n}^{-p} = G_{m-n}^{(-q,-1)}(\mathbf{0},\beta_x) + \sigma_{n-m}(\beta_x) + G_{m-n}^{(1,\infty)}(\mathbf{0},\beta_x) \tag{162}$$

$$= \tau_{m-n}(\boldsymbol{\beta}) - G_{m-n}^{(-\infty,-q-1)}(\mathbf{0},\beta_x) \tag{163}$$

and utilising the dispersion relation (91). Thus, we obtain

$$\hat{A}_n^q + Z_n \sum_{m=-\infty}^{\infty}\sum_{p=0}^{\infty} \hat{A}_m^p S_{m-n}^{q-p}(k\cos\psi_0) = T_n^q + Z_n \sum_{m=-\infty}^{\infty} B_m e^{iq\mathbf{s}_2\cdot\boldsymbol{\beta}} G_{m-n}^{(-\infty,-q-1)}(\mathbf{0},\boldsymbol{\beta}). \tag{164}$$

Similarly, if we substitute the decomposition (83) for multiple Bloch waves into the system (81), moving terms involving Bloch waves to the right hand side and simplifying, we find that

$$\hat{A}_n^q + Z_n \sum_{m=-\infty}^{\infty}\sum_{p=0}^{\infty} \hat{A}_m^p S_{m-n}^{q-p}(k\cos\psi_0) = T_n^q + Z_n \sum_{m=-\infty}^{\infty}\sum_{\mu=1}^{\lambda} B_m^{(\mu)} e^{iq\mathbf{s}_2\cdot\boldsymbol{\beta}^{(\mu)}} G_{m-n}^{(-\infty,-q-1)}(\mathbf{0},\boldsymbol{\beta}^{(\mu)}). \tag{165}$$

5.3 Reflection and Transmission

In terms of scattering angles ψ_j, we have

$$k\cos\psi_j = k\cos\psi_0 + 2j\pi/s_1 \qquad \text{and} \qquad k\sin\psi_j = i\gamma(k\cos\psi_j), \tag{166}$$

so that $\beta_{xj} = k\cos\psi_j$, and the spectral forms (39), (46) and (47) of the Green's functions can be written as [19]

$$G_n(\mathbf{r},\beta_x) = \frac{2(-i)^n}{ks_1}\sum_{j=-\infty}^{\infty}\frac{e^{in\,\mathrm{sgn}(y)\psi_j}}{\sin\psi_j}e^{ik(x\cos\psi_j+|y|\sin\psi_j)}, \tag{167}$$

$$G_n^{(q_0,\infty)}(\mathbf{r},\boldsymbol{\beta}) = \frac{2(-i)^n}{ks_1}\sum_{j=-\infty}^{\infty}\tau_j^{-q_0}e^{iq_0\boldsymbol{s}_2\cdot\boldsymbol{\beta}}\frac{e^{ik(x\cos\psi_j-y\sin\psi_j)}}{\sin\psi_j(1-\tau_j^{-1}e^{i\mathbf{s}_2\cdot\boldsymbol{\beta}^{(m)}})}e^{-in\psi_j}, \qquad y\le q_0\eta_2, \tag{168}$$

and

$$G_n^{(-\infty,q_1)}(\mathbf{r},\boldsymbol{\beta}) = \frac{2(-i)^n}{ks_1}\sum_{j=-\infty}^{\infty}\rho_j^{q_1}e^{iq_1\boldsymbol{s}_2\cdot\boldsymbol{\beta}}\frac{e^{ik(x\cos\psi_j+y\sin\psi_j)}}{\sin\psi_j(1-\rho_j^{-1}e^{-i\mathbf{s}_2\cdot\boldsymbol{\beta}^{(m)}})}e^{in\psi_j}, \qquad y\ge q_1\eta_2. \tag{169}$$

Recall the definitions (138) of τ_j and ρ_j from Section 4.4.

Now, the total field between two consecutive rows expanded as a series of grating modes therefore takes the form

$$u(\mathbf{r}) = \sum_{j=-\infty}^{\infty}e^{ikx\cos\psi_j}\left[c_{jq}^{-}e^{-iky\sin\psi_j}+c_{jq}^{+}e^{iky\sin\psi_j}\right], \qquad (q-1)\eta_2\le y\le q\eta_2. \tag{170}$$

Below the lattice, we have

$$u(\mathbf{r}) = e^{ik(x\cos\psi_0+y\sin\psi_0)}+\sum_{j=-\infty}^{\infty}c_{j0}^{-}e^{ik(x\cos\psi_j-y\sin\psi_j)}, \qquad y\le 0, \tag{171}$$

where the first term on the right-hand side represents the incident field, and the second contains only downward propagating modes. In terms of quasiperiodic Green's functions, the scattered field is given by

$$u^s(\mathbf{r}) = \sum_{n=-\infty}^{\infty}\sum_{p=0}^{\infty}A_n^pG_n(\mathbf{r}-p\mathbf{s}_2,\beta_x), \tag{172}$$

or, using the decomposition (83) and quasiperiodicity,

$$\begin{aligned} u^s(\mathbf{r}) &= \sum_{n=-\infty}^{\infty}\sum_{p=0}^{\infty}\left[\hat{A}_n^pG_n(\mathbf{r}-p\mathbf{s}_2,\beta_x)+\sum_{m=1}^{\lambda}B_n^{(m)}e^{ip\mathbf{s}_2\cdot\boldsymbol{\beta}^{(m)}}G_n(\mathbf{r}-p\mathbf{s}_2,\beta_x)\right] \\ &= \sum_{n=-\infty}^{\infty}\left[\sum_{p=0}^{\infty}\hat{A}_n^pG_n(\mathbf{r}-p\mathbf{s}_2,\beta_x)+\sum_{m=1}^{\lambda}B_n^{(m)}G_n^{(0,\infty)}(\mathbf{r},\boldsymbol{\beta})\right]. \end{aligned} \tag{173}$$

Next, we use the series expansions (167) and (168) of the Green's functions with $y < 0$ to obtain the reflection coefficient

$$c_{j0}^{-} = \sum_{n=-\infty}^{\infty} \frac{2(-i)^n e^{-in\psi_j}}{ks_1 \sin\psi_j} \left[\sum_{m=1}^{\lambda} \frac{B_n^{(m)} \tau_j}{(\tau_j - e^{i\mathbf{s}_2 \cdot \boldsymbol{\beta}^{(m)}})} + \sum_{p=0}^{\infty} \hat{A}_n^p \tau_j^{-p} \right]. \tag{174}$$

To calculate the transmission coefficients, we first split the total field $u = u^i + u^s$ into decaying and non-decaying parts,

$$u(\mathbf{r}) = \hat{u}(\mathbf{r}) + u^b(\mathbf{r}), \tag{175}$$

where

$$\hat{u}(\mathbf{r}) = e^{ik(x\cos\psi_0 + y\sin\psi_0)} + \sum_{n=-\infty}^{\infty} \left[\sum_{p=0}^{\infty} \hat{A}_n^p G_n(\mathbf{r} - p\mathbf{s}_2, \beta_x) - \sum_{m=1}^{\lambda} B_n^{(m)} G_n^{(-\infty,-1)}(\mathbf{r}, \boldsymbol{\beta}^{(m)}) \right], \tag{176}$$

and

$$u^b(\mathbf{r}) = \sum_{n=-\infty}^{\infty} \sum_{m=1}^{\lambda} B_n^{(m)} G_n^{(-\infty,\infty)}(\mathbf{r}, \boldsymbol{\beta}^{(m)}). \tag{177}$$

If we first consider downward propagating modes of (176), we only have contributions from the central term on the right-hand side. Hence, using the series expansion (167) of $G_n(\mathbf{r} - p\mathbf{s}_2, \beta_x)$ with $y < p\eta_2$, we see that

$$\hat{c}_{jq}^{-} = \sum_{n=-\infty}^{\infty} \frac{2(-i)^n}{ks_1} \frac{e^{-in\psi_j}}{\sin\psi_j} \sum_{p=q}^{\infty} \hat{A}_n^p \tau_j^{-p}. \tag{178}$$

To obtain an expression for $\hat{c}_j^{+}$, we require contributions from all three terms on the right-hand side of (176). From the central term, we have $y > p\eta_2$ and hence the expansion takes the form

$$\sum_{n=-\infty}^{\infty} \frac{2(-i)^n}{ks_1} \sum_{p=0}^{q-1} \hat{A}_n^p \sum_{j=-\infty}^{\infty} \frac{e^{in\psi_j}}{\sin\psi_j} e^{ik(x\cos\psi_j + y\sin\psi_j)} \rho_j^p. \tag{179}$$

From the third term on the right-hand side, we have

$$\sum_{n=-\infty}^{\infty} \frac{2(-i)^n}{ks_1} \sum_{m=1}^{\lambda} B_n^{(m)} \sum_{j=-\infty}^{\infty} \frac{e^{in\psi_j}}{\sin\psi_j (\rho_j e^{is_2 \cdot \beta^{(m)}} - 1)} e^{ik(x\cos\psi_j + y\sin\psi_j)}, \tag{180}$$

and hence we find that

$$\hat{c}_{jq}^{+} = \delta_{j0} + \sum_{n=-\infty}^{\infty} \frac{2(-i)^n e^{in\psi_j}}{ks_1 \sin\psi_j} \left[\sum_{p=0}^{q-1} \hat{A}_n^p \rho_j^p + \sum_{m=1}^{\lambda} \frac{B_n^{(m)}}{1 - \rho_j e^{is_2 \cdot \beta^{(m)}}} \right]. \tag{181}$$

For the contributions from Bloch waves, we have

$$u^b(\mathbf{r}) = \sum_{j=-\infty}^{\infty} e^{ikx\cos\psi_j} \left[c_{jq}^{b-} e^{-iky\sin\psi_j} + c_{jq}^{b+} e^{iky\sin\psi_j} \right], \tag{182}$$

and so, upon using (177) and (168) with $q_0 = q = q_1 + 1$, we see that

$$c_{jq}^{b-} = \sum_{n=-\infty}^{\infty} \frac{2(-i)^n \tau_j^{-q} e^{-in\psi_j}}{ks_1 \sin\psi_j} \sum_{m=1}^{\lambda} \frac{B_n^{(m)} e^{iq\boldsymbol{s_2}\cdot\boldsymbol{\beta}^{(m)}}}{1 - \tau_j^{-1} e^{i\boldsymbol{s_2}\cdot\boldsymbol{\beta}^{(m)}}}. \tag{183}$$

For upwards propagating modes, we use (169) and hence obtain

$$c_{jq}^{b+} = \sum_{n=-\infty}^{\infty} \frac{2(-i)^n \rho_j^q e^{in\psi_j}}{ks_1 \sin\psi_j} \sum_{m=1}^{\lambda} \frac{B_n^{(m)} e^{iq\mathbf{s}_2\cdot\boldsymbol{\beta}^{(m)}}}{\rho_j e^{i\boldsymbol{s_2}\cdot\boldsymbol{\beta}^{(m)}} - 1}. \tag{184}$$

Now, analysis from studying this problem using the Wiener-Hopf method (see [16]) yields the result that only Bloch waves are present in the far-field. Hence, by considering (181) for propagating modes, we see that

$$\delta_{j0} + \sum_{n=-\infty}^{\infty} \frac{2(-i)^n e^{in\psi_j}}{ks_1 \sin\psi_j} \left[\sum_{p=0}^{\infty} \hat{A}_n^p \rho_j^p + \sum_{m=1}^{\lambda} \frac{B_n^{(m)}}{1 - \rho_j e^{is_2\cdot\beta^{(m)}}} \right] = 0, \qquad j \in \mathcal{M}. \tag{185}$$

This provides us with a test for the accuracy of the coefficients found using this method.

6 Conservation of Energy

The problem of excitation of Bloch waves satisfies the conservation of energy condition derived in [18], which involves evaluating the integral

$$\langle E_S \rangle = -\frac{P_0\omega}{2} \Im \int_S u(\mathbf{r}) \frac{\partial}{\partial n} u^*(\mathbf{r}) \, \mathrm{d}s, \tag{186}$$

around a parallelogram S with vertices at

$$r = \pm\frac{1}{2}\mathbf{s_1} \pm (N + \frac{1}{2})\mathbf{s_2}, \qquad N \in \mathbb{N}, \tag{187}$$

taking the derivative in the direction of the outgoing normal at each side. Let S_1 denote the side of S that is below the lattice, S_2 the upper edge of S, and E_i denote $\langle E_{S_i} \rangle$, so that $\langle E_S \rangle = E_1 + E_2$ (it is shown in [18] that the sum of the integrals along the other two sides of S equals zero). Hence, we require $\langle E_S \rangle = 0$ to show that the energy is conserved.

For the edge below the lattice, we evaluate the simplified form (35) of (186) for the reflected field (174), taking the normal derivative in the $-\hat{\mathbf{y}}$ direction. After simplifications, we have

$$E_1 = -\frac{P_0 \omega k s_1}{2} \left[\sin\psi_0 - \sum_{j \in \mathcal{M}'} \sin\psi_j |c_{j0}^-|^2 \right]. \tag{188}$$

For the case where Bloch waves are excited, we have $E_1 < 0$ and

$$E_1 + E_2 = 0 \tag{189}$$

where E_2 is the average energy flux across the upper edge of the parallelogram, determined by evaluating (31) using the Bloch amplitude coefficients (183) and (184). Inserting (188) into (189)and simplifying, we obtain

$$\frac{1}{\sin\psi_0} \sum_{j \in \mathcal{M}'} \sin\psi_j |c_{j0}^-|^2 + \frac{2E_2}{P_0 \omega k s_1 \sin\psi_0} = 1, \tag{190}$$

where the first term on the left-hand side represents the proportion of reflected energy, and the second term is the proportion of transmitted energy. Hence, calculation of E_2 is unnecessary, however evaluating the left-hand side of (190) provides us with a further test of the accuracy of our results.

In the absence of Bloch waves, $E_1 = 0$ so that

$$\frac{1}{\sin\psi_0} \sum_{j \in \mathcal{M}'} \sin\psi_j |c_{j0}^-|^2 = 1. \tag{191}$$

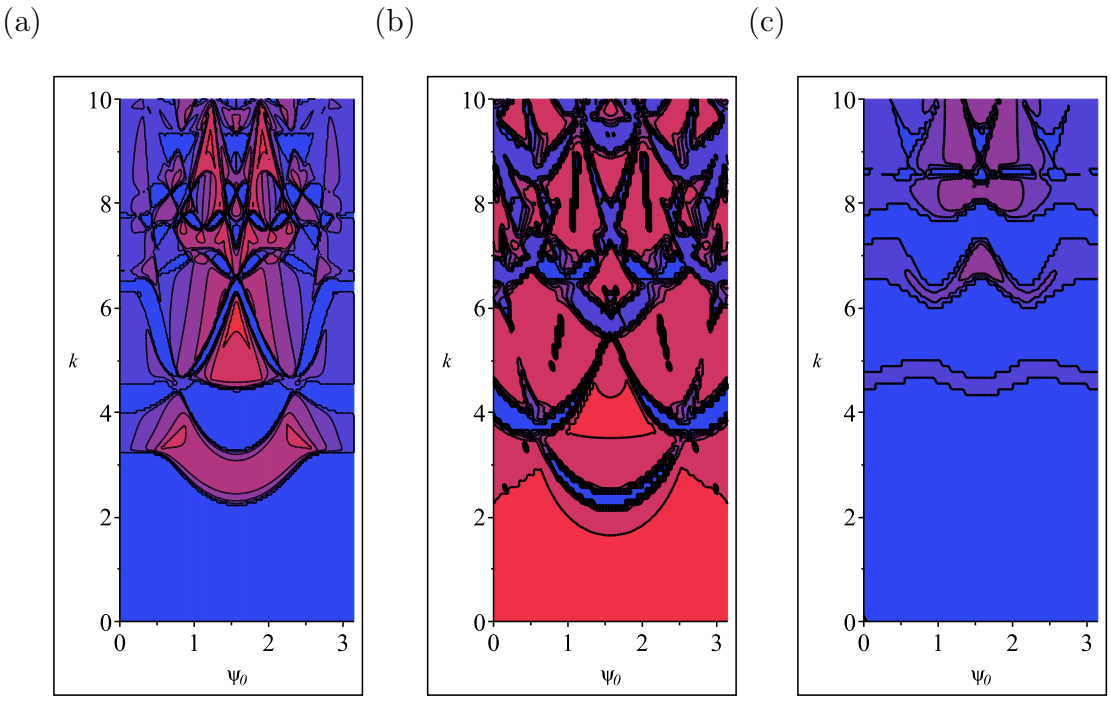

Figure 4: Contour plots showing the proportion of reflected energy for varying frequency and angle of incidence. (a) $\mathbf{s}_1 = [1, 0]$, $\mathbf{s}_2 = [0, 1]$, $a = 0.1$, Dirichlet boundary conditions. (b) as (a), but with Neumann boundary conditions. (c) $\mathbf{s}_1 = [1, 0]$, $\mathbf{s}_2 = [0.25, 1]$, $a = 0.3$, Dirichlet boundary conditions.

7 Results

Having found all amplitude coefficients for the reflected and transmitted fields in Section 5.3, we now use (190) to calculate the proportion of the incident field that is reflected back from the lattice, and demonstrate the results using contour plots, since these show more information than band diagrams. Contour plots in figures 4 onwards show band gaps, as well as the amound of energy that is transmitted into the lattice, which cannot be determined from a band diagram. Band diagrams corresponding to figures 6 and 7 can be found in [12].

Figures 4-11 show the proportion of reflected energy for various lattice con-

(a) (b) (c)

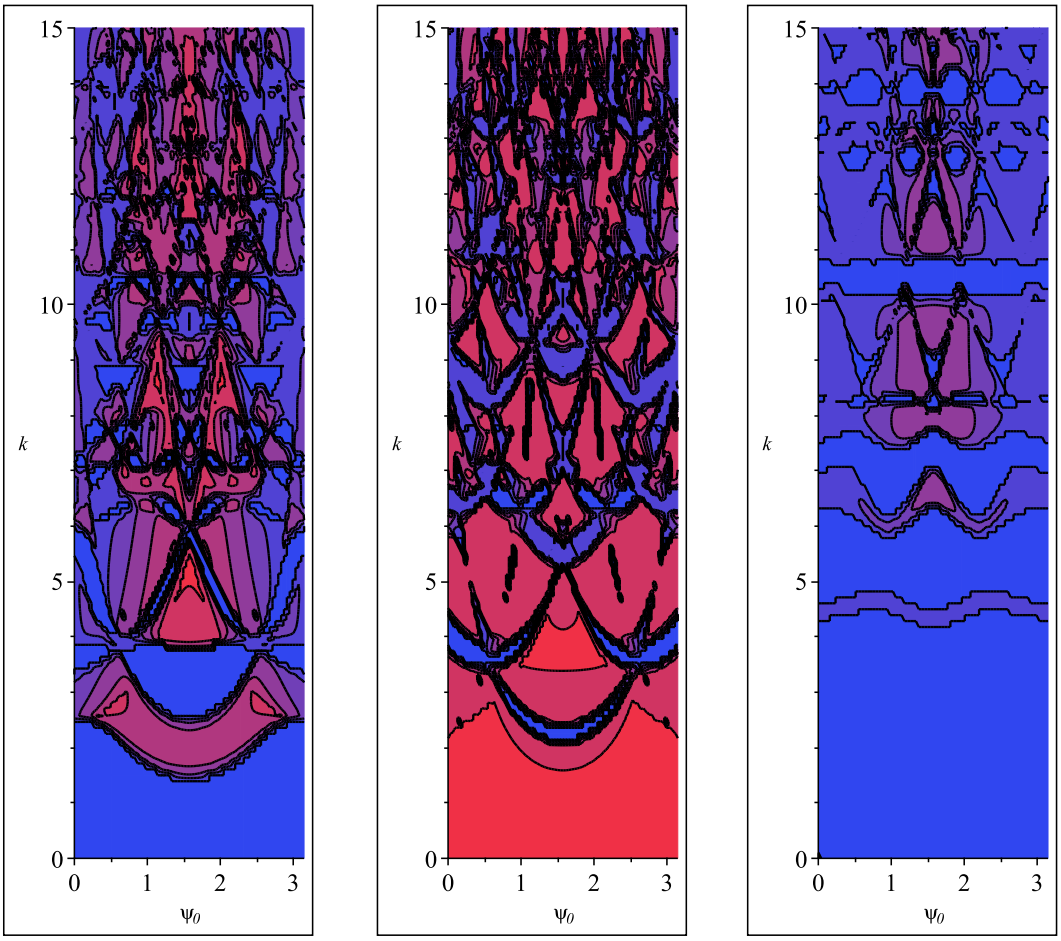

Figure 5: Contour plots showing the proportion of reflected energy for varying frequency and angle of incidence. (a) $\mathbf{s}_1 = [1, 0]$, $\mathbf{s}_2 = [0, 1]$, $a = 0.1$, Dirichlet boundary conditions. (b) as (a), but with Neumann boundary conditions. (c) $\mathbf{s}_1 = [1, 0]$, $\mathbf{s}_2 = [0.25, 1]$, $a = 0.3$, Dirichlet boundary conditions.

figurations. In each case, $\mathbf{s}_1 = [1, 0]$, and the angle of incidence is varied so that $0 < \psi_0 < \pi$. Red regions represent low reflection, whereas blue regions represent high reflection, and hence low transmission. All of the results satisfy the conservation of energy condition (189) and the far-field condition (185). Typically, methods for solving time-harmonic wave scattering problems increase in computational difficulty as the frequency increases. Our new method found no such difficulties for larger k values.

Figure 4 shows contour plots of the proportion of reflected energy, with parameters used in [19], so that we can compare results for verification that the filtering method works. Figures 4(a) and 4(b) show the reflected energy for a square lattice, with $\mathbf{s}_2 = [0, 1]$, $a = 0.1$, varying the frequency so that $0 < k < 10$, with Dirichlet and Neumann boundary conditions, respectively. In figure 4(c), $a = 0.3$, Dirichlet boundary conditions are used, and the lattice is skewed by setting $\mathbf{s}_2 = [0.25, 1]$. These results are all in agreement with figures 4(a) , 5(a), and 7(c) in [19].

Figures 5(a)–(c) show contour plots of the proportion of reflected energy using the same parameters as figures 4(a)–(c), respectively, but this time with $0 < k < 15$. We see that very complex patterns occur at high frequencies in figures 5(a) and 5(b), with no total band gaps, except the low frequency gap in 5(a). Total band gaps are evident in figure 5(c), for $k \lesssim 5.2$, $4.9 \lesssim k \lesssim 5.8$ $7.0 \lesssim k \lesssim 7.5$ and $10.3 \lesssim k \lesssim 10.5$. However, transmission in other parameter regimes is low, so this structure would not make a good band gap filter.

Figures 6 and 7 demonstrate the proportion of reflected energy using parameter regimes as in [12]. This paper was concerned with whether transmission is possible, rather than how much transmission occurs, whereas here we have obtained more quantitive data. Figures 6(a) and 7(a) correspond to the parameters in figure 3 of [12]; thus $\mathbf{s}_2 = [0, 1]$ and $a = 0.26$. In figure 6(a), we have Neumann boundary conditions (called p polarization in [12]), and we can see mostly transmission until

(a) (b) (c)

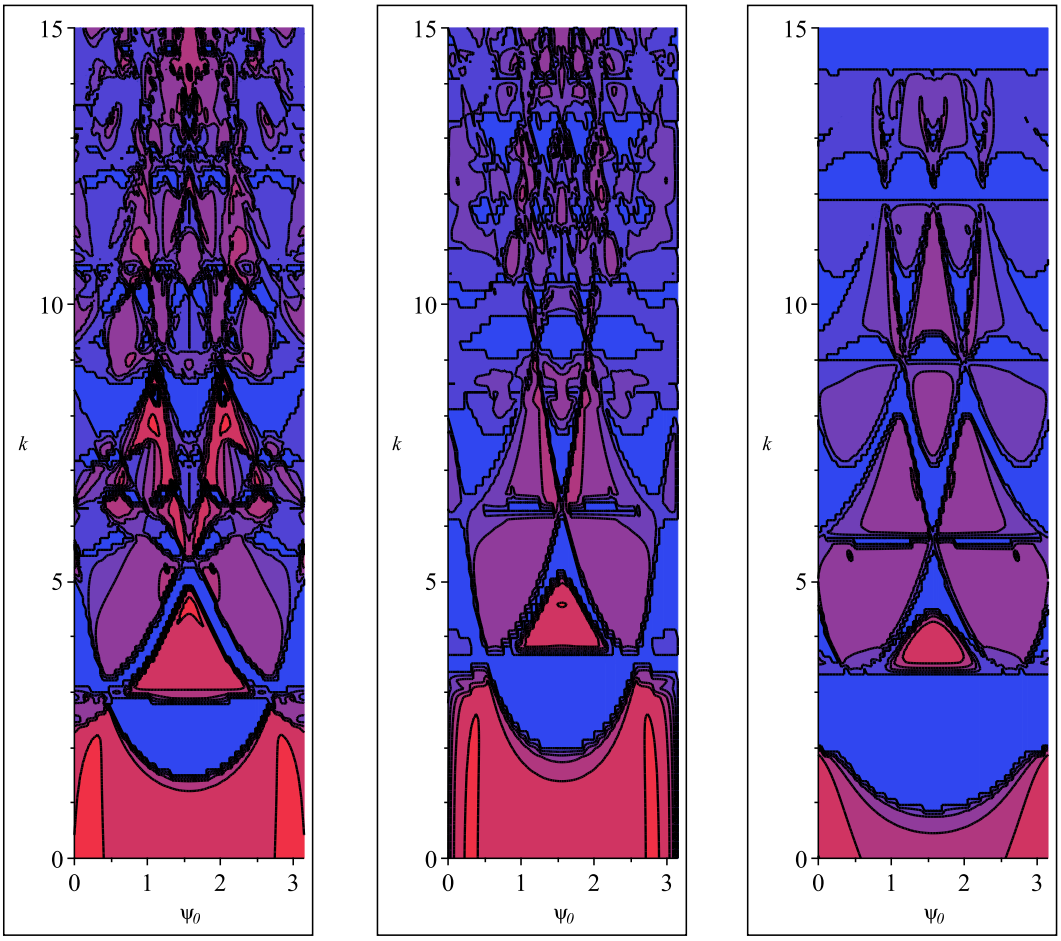

Figure 6: Contour plots showing the proportion of reflected energy for varying frequency and angle of incidence. (a) $\mathbf{s}_1 = [1, 0]$, $\mathbf{s}_2 = [0, 1]$, $a = 0.26$, Neumann boundary conditions. (b) as (a), but with $a = 0.34$ (c) as (a), but with $a = 0.42$

(a) (b)

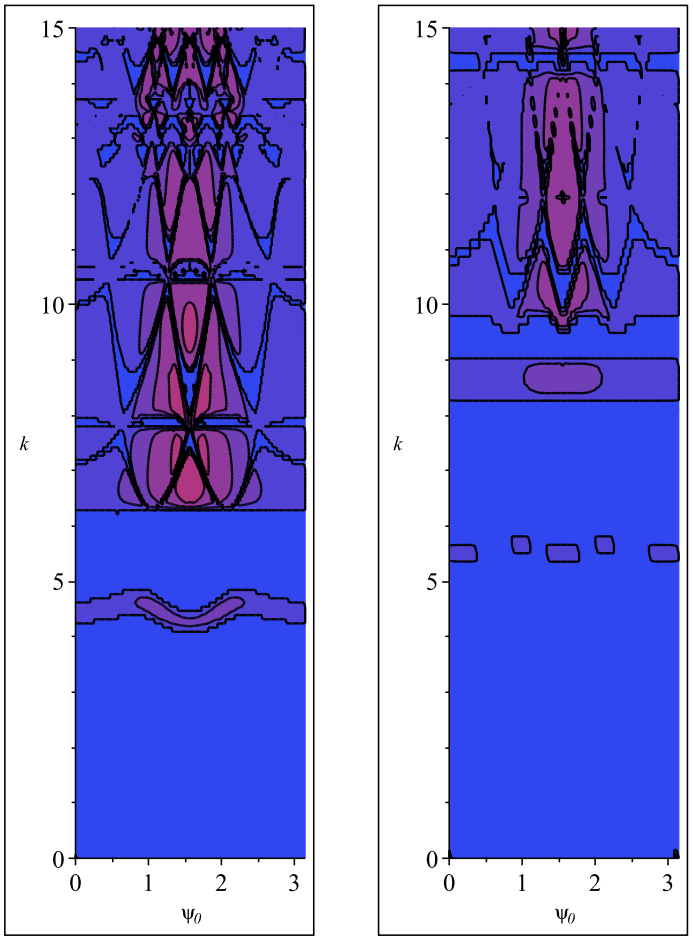

Figure 7: Contour plots showing the proportion of reflected energy for varying frequency and angle of incidence. (a) $\mathbf{s}_1 = [1, 0]$, $\mathbf{s}_2 = [0, 1]$, $a = 0.26$, Dirichlet boundary conditions. (b) as (a), but with $a = 0.34$

$k \approx 3$, after which the plot becomes increasingly convoluted as k increases, with no total band-gaps. Overall, the transmission is low at higher frequencies, a fact which cannot be deduced from an ordinary band diagram. In figure 7(a), we have Dirichlet conditions (called s polarization in [12]). As predicted in [12], there is a band gap for $k \lesssim 4.2$, followed by a narrow band in which transmission is possible, and then a second gap for $\lesssim 4.9k \lesssim 6.2$. Within the regions where transmission is possible, the amount of reflection is generally very high, so again this structure would not be effective as a band gap filter. In figures 6(b) and 7(b), the scatterer radius has been increased to 0.34, as in figure 4 of [12]. For Neumann boundary conditions (figure 6(b)), a narrow band gap is evident at $k \approx 3.5$, as predicted in [12]. For Dirichlet conditions (figure 7(b)), the pattern is similar to the case with $a = 0.26$, but the bands are shifted upwards. A third gap has now appeared, between $k \approx 9$ and $k \approx 9.6$. This is not shaded in figure 4 of [12], but it is evident from a careful study of the figure. For Neumann conditions with $a = 0.42$ (figure 6(c)), a band gap is evident for $2 \lesssim k \lesssim 3.3$. The lower edge of this gap does not agree with the value shown in figure 4 of [12], but this can be accounted for by the fact that $-\pi/s_1 < \beta_x < \pi/s_1$ within the Brillouin zone, but here we have $\beta_x = k \cos\psi_0$, so that $-k < \beta_x < k$. Consequently, for $k < \pi$, there may be Bloch waves that cannot be excited by any incident plane wave. For Dirichlet conditions with $a = 0.42$, we found almost total reflection for all parameters, so no plot for this case is shown.

Figures 8 and 9 show the proportion of reflected energy with $0 < k < 20$ using different parameters. Dirichlet boundary conditions are applied in figure 8, and Neumann conditions in figure 9. In figure 8(a), we have $a = 0.42$ and $\mathbf{s}_2 = [0, 1]$. Here we see that almost all energy is reflected, with no transmission occurring until $k \approx 13.5$, after which there are three narrow pass bands at $13.5 \lesssim k \lesssim 13.6$, $15.1 \lesssim k \lesssim 15.2$ and $16.8 \lesssim k \lesssim 17.2$. There is a wider pass band for $k > 19$, but

(a) (b)

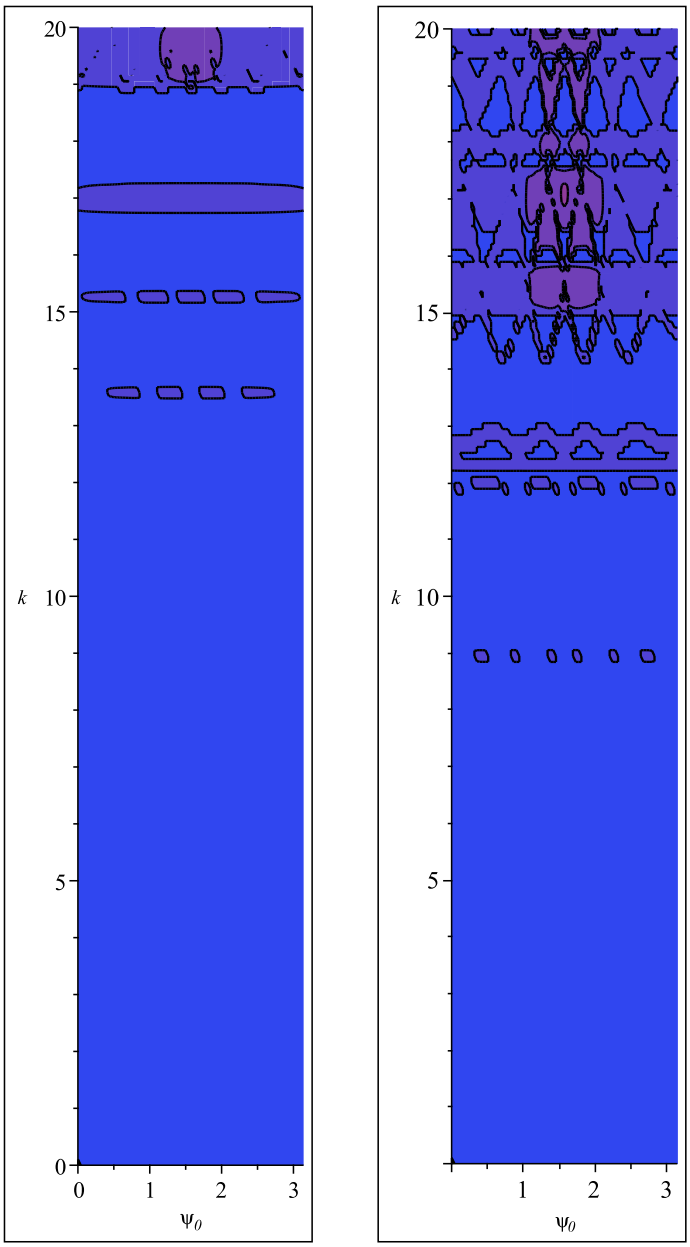

Figure 8: Contour plots showing the proportion of reflected energy for varying frequency and angle of incidence. (a) $\mathbf{s}_1 = [1, 0]$, $\mathbf{s}_2 = [0, 1]$, $a = 0.42$, Dirichlet boundary conditions. (b) $\mathbf{s}_1 = [1, 0]$, $\mathbf{s}_2 = [0.25, 1]$, $a = 0.4$, Dirichlet boundary conditions.

(a) (b)

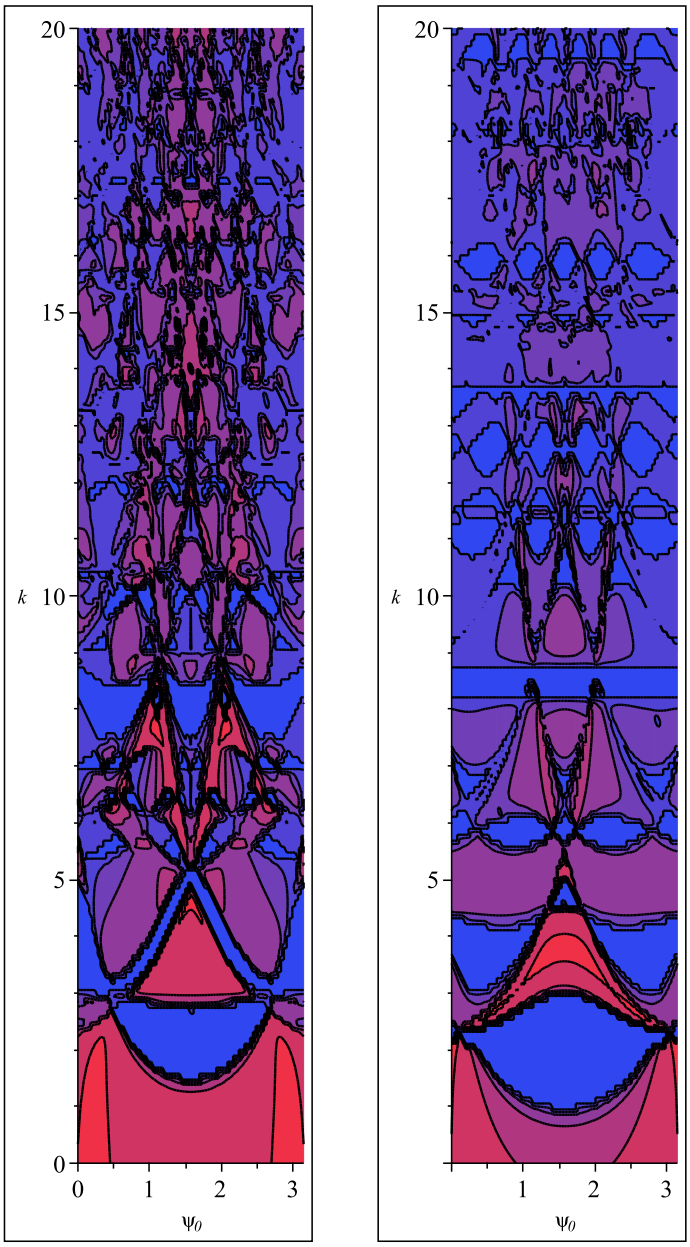

Figure 9: Contour plots showing the proportion of reflected energy for varying frequency and angle of incidence. (a) $\mathbf{s}_2 = [0, 1]$, $a = 0.25$, Neumann boundary conditions. (b) $\mathbf{s}_2 = [0.25, 1], a = 0.4$.

in all cases the proportion of transmitted energy is very low. In figure 8(b), the lattice is skewed, with parameters $a = 0.4$ and $\mathbf{s}_2 = [0.25, 1]$. Again, almost all of the incident energy is reflected back from the lattice. Very low transmission occurs at $k \approx 6.8$, but only for certain angles of incidence. There is a more extensive pass band for $8.9 \lesssim k \lesssim 9.9$, and for $k \gtrsim 11$ the structure permits transmission in most directions, but again the proportion of transmitted energy is very low. Figure 9(a) uses parameters $a = 0.25$ and $\mathbf{s}_2 = [0, 1]$, and for figure 9(b) we have $a = 0.4$ and $\mathbf{s}_2 = [0.25, 1]$. In both cases, there is strong transmission at low frequencies, and a region of strong reflection centred around head-on incidence for $1.5 \lesssim k \lesssim 3$. At higher frequencies the patterns become increasingly complex. No total band gaps are evident in figure 9(a). Overall, there is more reflection in figure 9(b), and in particular, a narrow total band gap is evident at $k \approx 8.5$.

Figures 8 and 9 show the proportion of reflected energy with $0 < k < 20$ using different parameters. Dirichlet boundary conditions are applied in figure 8, and Neumann conditions in figure 9. In figure 8(a), we have $a = 0.42$ and $\mathbf{s}_2 = [0, 1]$. Here we see that almost all energy is reflected, with no transmission occurring until $k \approx 13.5$, after which there are three narrow pass bands at $13.5 \lesssim k \lesssim 13.6$, $15.1 \lesssim k \lesssim 15.2$ and $16.8 \lesssim k \lesssim 17.2$. There is a wider pass band for $k > 19$, but in all cases the proportion of transmitted energy is very low. In figure 8(b), the lattice is skewed, with parameters $a = 0.4$ and $\mathbf{s}_2 = [0.25, 1]$. Again, almost all of the incident energy is reflected back from the lattice. Very low transmission occurs at $k \approx 6.8$, but only for certain angles of incidence. There is a more extensive pass band for $8.9 \lesssim k \lesssim 9.9$, and for $k \gtrsim 11$ the structure permits transmission in most directions, but again the proportion of transmitted energy is very low. Figure 9(a) uses parameters $a = 0.25$ and $\mathbf{s}_2 = [0, 1]$, and for figure 9(b) we have $a = 0.4$ and $\mathbf{s}_2 = [0.25, 1]$. In both cases, there is strong transmission at low frequencies, and a region of strong reflection centred around head-on incidence for $1.5 \lesssim k \lesssim 3$. At

(a) (b)

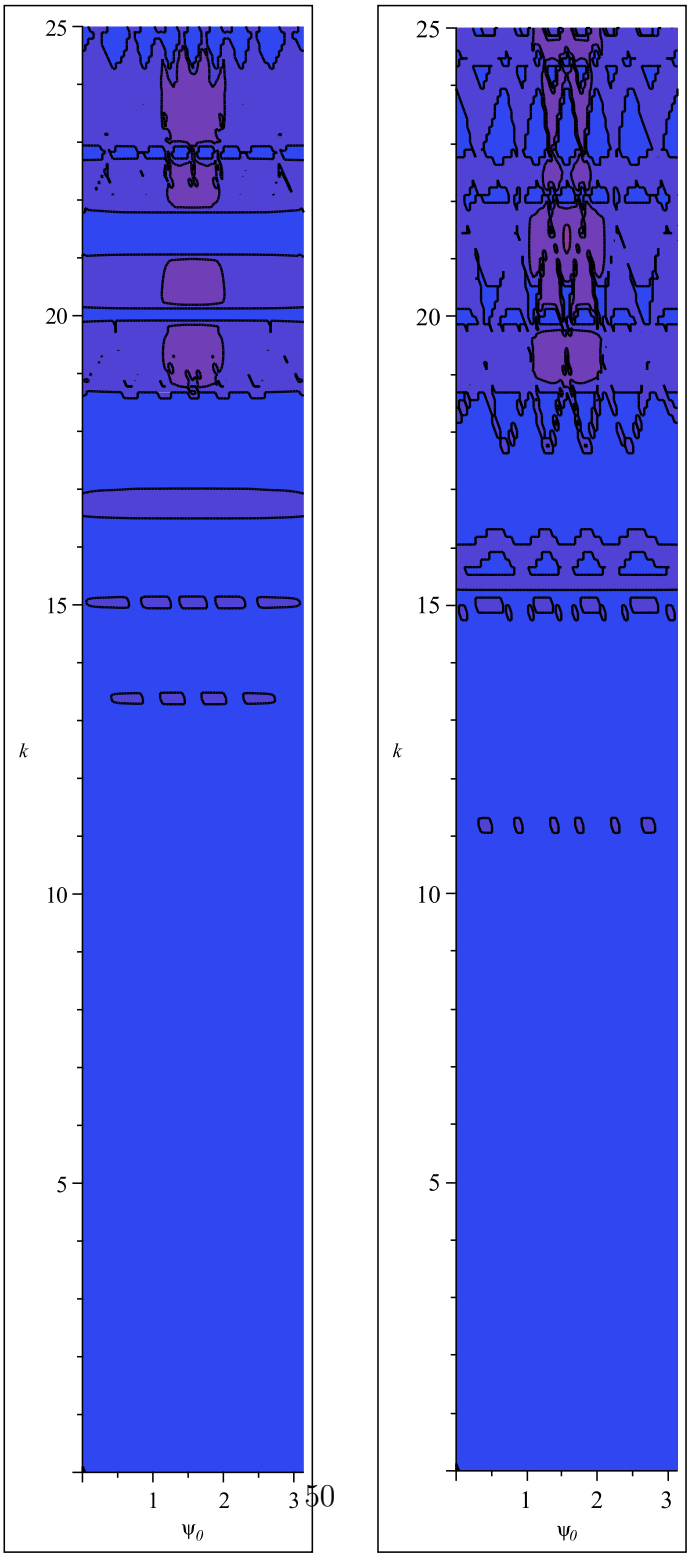

Figure 10: Contour plots showing the proportion of reflected energy for varying frequency and angle of incidence. (a) $\mathbf{s}_1 = [1, 0]$, $\mathbf{s}_2 = [0, 1]$, $a = 0.42$, Dirichlet boundary conditions. (b) $\mathbf{s}_1 = [1, 0]$, $\mathbf{s}_2 = [0.25, 1]$, $a = 0.4$, Dirichlet boundary conditions.

(a) (b)

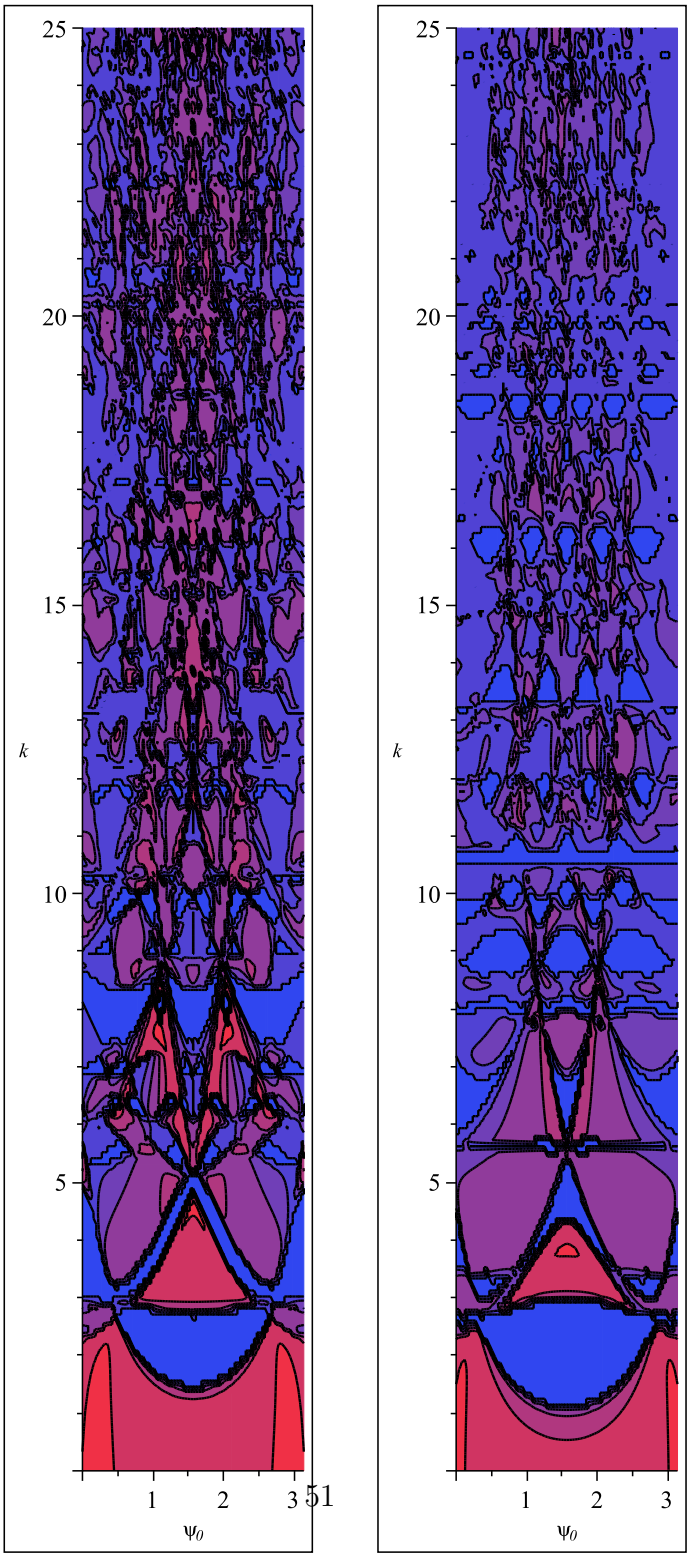

Figure 11: Contour plots showing the proportion of reflected energy for varying frequency and angle of incidence. (a) $\mathbf{s}_1 = [1, 0]$, $\mathbf{s}_2 = [0, 1]$, $a = 0.25$, Neumann boundary conditions. (b) $\mathbf{s}_1 = [1, 0]$, $\mathbf{s}_2 = [0.1, 1]$, $a = 0.35$, Neumann boundary conditions.

higher frequencies the patterns become increasingly complex. No total band gaps are evident in figure 9(a). Overall, there is more reflection in figure 9(b), and in particular, a narrow total band gap is evident at $k \approx 8.5$.

In figures 10 and 11, the range of frequencies increased further so that now $0 < k < 25$. Dirichlet boundary conditions are used in figure 10, with $a = 0.42$ and $\mathbf{s}_2 = [0, 1]$ for figure 10(a), and $a = 0.4$ and $\mathbf{s}_2 = [0.25, 1]$ for figure 10(b). The patterns are similar to those shown in figure 8, with reflection the dominant effect. There are more complex patterns at high frequencies, and pass bands in both plots, but the proportion of transmitted energy is always low. Neumann boundary conditions are used in figures 9(a) and (b), with $a = 0.25$ and $\mathbf{s}_2 = [0, 1]$, and $a = 0.35$ and $\mathbf{s}_2 = [0.1, 1]$, respectively. The patterns are similar to those shown in figure 9, with high transmission at low frequencies, and very complex patterns at higher frequencies. There is a very narrow band gap in figure 9(a), at $k \approx 10.5$; no total band gaps are evident in figure 9(b).

8 Concluding Remarks

We have developed a new method for modelling the reflection and transmission that occurs when a plane wave hits the edge of a semi-infinite lattice. The method avoids the use of integral transforms and the Wiener-Hopf technique. Both our method and the Wiener-Hopf method require the solution to the associated propagation problem, in order to determine the parameters for any Bloch waves that may be excited. The Wiener–Hopf method also requires information about the zeros of a function called the *kernel*, as well as factorisation of the kernel into a product of analytic functions inside and outside the unit circle. In contrast, the new method only requires the numerical solution of a rapidly convergent, infinite linear system of algebraic equations.

Initially, we considered the simple case in which the lattice is composed from point scatterers, and this was used to demonstrate the effectiveness and accuracy of our method. We then moved on to introduce finite size effects. In this case, solving via the Wiener–Hopf method as in [19] is complicated, and difficult to implement. However, our new method generalises to finite sized scatterers very easily, with the analysis almost identical to the point scatterer case, and more involved algebra being the only complication. This allowed us to consider a greater range of frequencies than those shown in [19], and to reproduce the results of [12], but showing the proportions of reflected and transmitted energy, not just the possibility of transmission. In general, we found that lattices composed of cylinders subject to Dirichlet boundary conditions allow limited transmission, particularly if the scatterer radius is large. In these cases, the high proportion of reflection in pass bands means that these structures could not be used to make efficient band gap filters. Lattices formed from cylinders subject to Neumann boundary conditions generally allow much greater transmission, but the patterns we observed at high frequencies are very complex, and a substantial proportion of incident energy is reflected at certain angles of incidence, even for parameters inside very wide pass bands.

Appendices

The function f defined as

$$f(z_1,\ldots,z_{\lambda+1}) = \sum_{m=1}^{\lambda}\prod_{\substack{n=1\\n\neq m}}^{\lambda}\frac{z_n - z_{\lambda+1}}{z_n - z_m} \tag{192}$$

is in fact the constant function $f(z_1,\ldots,z_{\lambda+1}) \equiv 1$.

Proof:

Firstly, consider fixed and distinct values for $z_2,\ldots,z_{\lambda+1}$, so that f is a function of one complex variable z_1. Then for any $p \in \{2,\ldots,\lambda\}$, $z_1 - z_p$ only appears in the denominator if $m = 1$ or $m = p$. If we separate out these terms and consider the limit as $z_1 \to z_p$, we find that

$$\lim_{z_1\to z_p}\left[\prod_{n=2}^{\lambda}\frac{z_n - z_{\lambda+1}}{z_n - z_1} + \prod_{\substack{n=1\\n\neq p}}^{\lambda}\frac{z_n - z_{\lambda+1}}{z_n - z_p}\right] = \prod_{\substack{n=1\\n\neq p}}^{\lambda}\frac{z_n - z_{\lambda+1}}{z_n - z_p}\lim_{z_1\to z_p}\left[\frac{z_p - z_{\lambda+1}}{z_p - z_1} + \frac{z_1 - z_{\lambda+1}}{z_1 - z_p}\right] \tag{193}$$

$$= \prod_{\substack{n=2\\n\neq p}}^{\lambda}\frac{z_n - z_{\lambda+1}}{z_n - z_p}. \tag{194}$$

Hence f is an entire function of z_1. Observing that

$$f(z_1,\ldots,z_{\lambda+1}) = \prod_{n=2}^{\lambda}\frac{z_n - z_{\lambda+1}}{z_n - z_1} + \sum_{m=2}^{\lambda}\frac{z_1 - z_{\lambda+1}}{z_1 - z_m}\prod_{\substack{n=2\\n\neq m}}^{\lambda}\frac{z_n - z_{\lambda+1}}{z_n - z_m}, \tag{195}$$

and therefore

$$\lim_{z_1\to\infty} f(z_1,\ldots,z_{\lambda+1}) = \sum_{m=2}^{\lambda}\prod_{\substack{n=2\\n\neq m}}^{\lambda}\frac{z_n - z_{\lambda+1}}{z_n - z_m}, \tag{196}$$

we see that f is a bounded entire function of z_1, and so by Liouville's theorem it must be independent of z_1 . The same result can be made replacing z_1 with z_n,

$n \in \{2, \ldots, \lambda\}$. To show that f is independent of $z_{\lambda+1}$, simply replace z_n with $z_n - \alpha$ for $n = 1, \ldots, \lambda$ in (192). Finally, setting $z_1 = z_{\lambda+1}$ in (192) so that the terms with $m > 1$ disappear, we obtain

$$f(z_1, \ldots, z_{\lambda+1}) = 1. \tag{197}$$

References

[1] Salvatore Campione, Matteo Albani, and Filippo Capolino. Complex modes and near-zero permittivity in 3d arrays of plasmonic nanoshells: loss compensation using gain. *Optical Materials Express*, 1(6):1077–1089, 2011.

[2] Huanyang Chen, Che Ting Chan, and Ping Sheng. Transformation optics and metamaterials. *Nature materials*, 9(5):387, 2010.

[3] DV Evans and R Porter. Flexural waves on a pinned semi-infinite thin elastic plate. *Wave Motion*, 45(6):745–757, 2008.

[4] PL Gourley, ME Warren, GA Vawter, TM Brennan, and BE Hammons. Optical bloch waves in a semiconductor photonic lattice. *Applied physics letters*, 60(22):2714–2716, 1992.

[5] Stewart G Haslinger, Alexander B Movchan, Natasha V Movchan, and Ross C McPhedran. Symmetry and resonant modes in platonic grating stacks. *Waves in Random and Complex Media*, 24(2):126–148, 2014.

[6] Norman L Hills and Samuel N Karp. Semi-infinite diffraction gratings—i. *Communications on pure and applied mathematics*, 18(1-2):203–233, 1965.

[7] A. Khelif, B. Aoubiza, S. Mohammadi, A. Adibi, and V. Laude. Complete band gaps in two-dimensional phononic crystal slabs. *Phys. Rev. E*, 74:046610, Oct 2006.

[8] Christopher M Linton and Philip McIver. *Handbook of mathematical techniques for wave/structure interactions*. CRC Press, 2001.

[9] CM Linton. Lattice sums for the helmholtz equation. *SIAM review*, 52(4):630–674, 2010.

[10] CM Linton, R Porter, and I Thompson. Scattering by a semi-infinite periodic array and the excitation of surface waves. *SIAM Journal on Applied Mathematics*, 67(5):1233–1258, 2007.

[11] PA Martin. *Multiple scattering: interaction of time-harmonic waves with N obstacles*, volume 107. Cambridge University Press, 2006.

[12] N. A. Nicorovici, R. C. McPhedran, and L. C. Botten. Photonic band gaps for arrays of perfectly conducting cylinders. *Phys. Rev. E*, 52:1135–1145, 1995.

[13] Benjamin Noble and George Weiss. Methods based on the wiener-hopf technique for the solution of partial differential equations. *Physics Today*, 12:50, 1959.

[14] FWJ Olver. *NIST handbook of mathematical functions hardback and CD-ROM*. Cambridge University Press, 2010.

[15] Arnold Sommerfeld. *Partial differential equations in physics*, volume 1. Academic press, 1949.

[16] V Twersky. On scattering of waves by the infinite grating of circular cylinders. *IRE Transactions on antennas and propagation*, 10(6):737–765, 1962.

[17] N Tymis and I Thompson. Low-frequency scattering by a semi-infinite lattice of cylinders. *The Quarterly Journal of Mechanics and Applied Mathematics*, 64(2):171–195, 2011.

[18] N Tymis and I Thompson. Scattering by a semi-infinite lattice and the excitation of bloch waves. *The Quarterly Journal of Mechanics and Applied Mathematics*, 67(3):469–503, 2014.